LUNDS UNIVERSITET

Master's Programme in Wireless Communication

ERICSSON

Performance evaluation and modeling of a beam-simulation system for MIMO communications

Master Thesis

by

Chen Linfeng
li7423ch-s@student.lu.se

ETIN02
Master's Thesis (30 credits ECTS)
2022
Supervisor: Peter Kornevi (Ericsson), Jens Grekula (Ericsson), Xuesong Cai (EIT)
Examiner: Michael Lentmaier

Abstract

For many years, communication systems that use beamforming technology to improve system performance in radio networks are evolving. Beamforming enables a mobile communication system to utilize the bandwidth efficiently and gain better coverage. Smart antenna-based beamforming technology can expand existing communication capacity by improving the Signal to Interference plus Noise Ratio (SINR). Advanced Antenna System (AAS) is a great example of smart antenna system that combines the antenna array and many multi-antenna features (such as beamforming) that can be implemented on the radio unit.

With the development of AAS, the requirement for its accuracy becomes stricter. The performance of AAS should be tested before being put into use, such as beamforming performance. Therefore, an efficient test system can effectively help the design of smart antennas. In this work, a beam simulation system based on the Butler matrix structure for beamforming testing was evaluated and verified. The assessment is carried out in two parts. The first part is the theoretical analysis and simulation of the expected measurement result. The second part is to measure the device and compare the results with the theoretical result. The target of this thesis is to evaluate the accuracy of this beam simulation system and make a proposal for improving Multiple Input Multiple Output (MIMO) feature verification.

Popular Science Summary

Since the 1980s, commercial wireless communications have rapidly evolved from simple voice systems to mobile broadband multimedia systems. The development of wireless communications has had a significant impact on daily lives. Due to the upgrade of mobile applications, the amount of data traffic and the number of wireless devices continue to increase. Current communication systems require complex signal processing techniques and flexible transmission schemes to achieve higher transmission speed in various environments. Compared to previous generation technologies (3G, 4G), 5G New Radio (NR) has significantly different performance criteria, including gigabit-per-second data rates, high traffic density, and millisecond-level low latency.

From the perspective of electromagnetic wave resources, the millimeter-wave frequency band has a large amount of unoccupied spectrum to transmit the data, making it a main frequency band for 5G NR. In the process of realizing 5G communication, the problem is that in the high-frequency band, especially the millimeter-wave band, the propagation loss of signal is large, which will lead to the reduction of the received signal power. The 5G radio equipped with multiple antennas can greatly ease this problem. In conventional radio system, the signal propagation is omnidirectional. By using multiple antennas, the signal can be concentrated to a direction, i.e., beamformed, to improve spatial coverage and power efficiency.

The performance of a radio system has to be comprehensively verified before deployment. Because beamforming technology needs to be implemented with high precision and reliability, beamforming testing is an important part of radio system verification. As an essential component of the beamforming test system, the beam simulation system has become a popular tool and research topic in the industry. In this thesis, we propose an innovative method to assess the validity of a beam simulation system and discuss how 5G verification can be benefited from this method.

Acronyms

3GPP 3^{rd} Generation Partnership Project
AAS Advanced Antenna System
BS Base Station
CCN Cellular Coaxial Network
CDM Code-Domain Sharing
CSI Channel State Information
CSI-RS Channel State Information Reference Signal
FDM Frequency-Domain Sharing
DCI Downlink Control Indicator
LTE Long-Term Evolution
MAC-CE Media Access Control Control Elements
MIMO Multiple Input Multiple Output
MU Multi-User
NR New Radio
OTA Over-The-Air
PA Planar Array
PDSCH Physical Downlink Shared Channel
PPRE Power per Resource Element
RF Radio Frequency
RB Resource Block
Rx Receiver
SER Symbol Error Rate
SINR Signal to Interference plus Noise Ratio
SISO Single Input Single Output
SRS Sounding Reference Signal
SSB Synchronization Signal Block
SU Single-User
TDM Time-Domain Sharing
Tx Transmitter
ULA Uniform Linear Array
UE User Equipment

Contents

List of Figures

List of Tables

1

Introduction

With the development of mobile communication technology, the number of User Equipment (UE) has risen significantly, which leads to severe spatial interference. The previous generation of communication system can no longer meet the demands of users. The new application scenarios require the communication system to have a higher transmission data rate, lower latency, and optimized power consumption. Therefore, the upgrade of the communication system has become a priority. The 3^{rd} Generation Partnership Project (3GPP) has launched the latest 5G NR standard in its Release 16 to supplement the 5G standard in many aspects. And Release 17 is almost completed and expected to be launched in 2022.

Beamforming is a key technology for the 5G network. For the MIMO beamforming verification in the corresponding development stage, it is a mandatory part to test the MIMO system on the external field channel. However, field testing is a time-consuming task. It requires a detailed test plan and experienced technicians to achieve comprehensive network verification. Therefore, the simulation of realistic channels in the laboratory has become an important and efficient test means in the early stage of the beamforming verification test. To improve the effectiveness of laboratory testing, many studies have been carried out in the past decade. For lab Over-The-Air (OTA) testing, [1] and [2] introduced a comparison test for MIMO OTA measurement methods standardization. In terms of test equipment, many researchers have proposed new OTA test system designs, such as [3]. Another common lab test is the conducted test. All the equipment of this system is connected by cables, which makes conducted test simpler and more economical than the OTA system. The core of conducted test is channel simulation. The 5G channel simulation tool provides a flexible and powerful Radio Frequency (RF) test environment that can simulate real beamforming field testing.

In this master thesis, the validity of a beam simulation system for MIMO system testing will be discussed along with the physical layer of the latest 5G standard.

1.1 Background

5G is a necessary prerequisite for emerging services and applications. First, 5G can further improve data rates and user experience based on existing mobile broadband service scenarios. 5G also makes new services possible, such as autonomous driving and Telehealth, that have extremely high requirements for latency and reliability. In addition, 5G can also support the large-scale Internet of Things. For example, it can meet the application requirements of smart home, environmental monitoring, etc. aiming at sensing and data collection.

To achieve reliable 5G communication, many performance requirements need to be considered. Some important performance parameters are mentioned in [4]. In signal transmission between Base Station (BS) and UE, high data rate and wide coverage area will be regarded as key requirements and top priorities. Communication at millimeter-wave frequency is the key technology of wireless transmission and can be used to effectively increase the data rate. For current 5G deployments, many of the devices operate on frequencies below 6 GHz, that is also known as the Sub 6G or FR1 band. This frequency band is suitable for wide area coverage. In short-range data traffic, in order to achieve higher-speed data transmission and larger channel capacity, 5G transmission will be carried out in the millimeter wave-frequency band FR2. FR1 ranges between 400 MHz and 7.125 GHz, and FR2 ranges between 24.250 GHz and 52.6 GHz.

With the advent of standards supporting faster data rates, wireless transmission systems have to be further modified to meet the new requirements. MIMO and Massive MIMO technologies are key techniques for improving the capacity and spectrum utilization of communication systems.

MIMO. MIMO system can implement multiple transmit and receive antennas at the transmitter and receiver, respectively. Signals are transmitted and received through multiple antennas at the transmitter and receiver, thereby improving communication quality. It can make full use of spatial diversity and achieve multiple transmissions and multiple receptions through multiple antennas, which can increase the system channel capacity without increasing bandwidth resource usage and power transmitted by the antenna. The space-time coding can help the MIMO system to achieve high power gain in signal transmission by transmitting different signal flows with time intervals larger than the time coherence of the channel. These signals are distributed over different frequencies and times. From the perspective of the radiation pattern, the radiation pattern of a multi-antenna system is the combination of the patterns from each single antenna element. Signal transmission is done using different polarization settings based on multi-path propagation of the MIMO system so that the receiver can receive individual signals. Therefore, with the benefit of space-time coding and spatial multiplexing, the MIMO system can achieve high-speed wireless communication [5] with a low Symbol Error Rate (SER).

Massive MIMO. The term "Massive MIMO" refers to an extension of MIMO which expands beyond the legacy system by equipping the base station with a much larger number of antennas. It can also be implemented at user terminals in some scenarios. The "massive" number of antennas helps the system focus energy in the target direction, enabling an extremely narrow beam, which brings a great boost in efficiency and throughput. As the number of antennas increases, both network devices and mobile devices implement more advanced designs to coordinate MIMO system operation. Under ideal conditions, every user equipment can share the same proportion of transmission power transmitted by the antennas at the BS. Antennas in Massive MIMO systems are digital antennas that can be used to provide diversity in BS and UE. The improvement of capacity requires the reduction of fading and interference. To achieve this goal, beamforming techniques can be deployed at the transmitter and receiver for signal transmission [6].

Beamforming is a technology that can help the system to generate a special radiation pattern to optimize system efficiency and energy consumption. It can be implemented at both transmitter and receiver with multiple antennas. The radiation pattern can be controlled within the capacity of beamforming. For example, the antenna array can generate a narrow, strong beam pointing toward the desired direction to provide the gain required

by UE. The principle of beamforming is to process the signal on each antenna according to the needs of the transmitter or receiver, including changing the amplitude and phase of the signal for each antenna. To make the antenna array focus the signal in certain directions and reduce the distribution of the signal in unwanted directions at the same time.

There are two types of beamforming: analog and digital. In analog beamforming, phased array circuits play an important role. Components in the circuit like phase shifters are used to control what signal the base station ultimately transmits. Digital beamforming is also known as precoding. In digital beamforming, multiple data streams are applied to each antenna with independent and appropriate weighting by the controller, better flexibility is achieved because different powers and phases can be assigned to the same antennas for different scenarios. This allows digital beamforming to play a key role in spatial multiplexing, where we want a superposition of transmitted signals, each with individual directivity. Digital and analog beamforming can be used together in the system, this is called hybrid beamforming. A MIMO system can generate a variety of beams by using beamforming such as precoding. These beams can be used to transmit data streams in different scenarios, such as Single-User (SU) MIMO and Multi-User (MU) MIMO. Both SU-MIMO and MU-MIMO improve system performance with multi-path propagation. A smart radio unit is required for the beamforming of the MIMO system. The radio unit we use is called Advanced Antenna System (AAS), which is powered by various multiple antenna technologies and algorithms.

AAS. AAS radio consists of an antenna array sophisticatedly integrated with the hardware and software required for transmitting and receiving radio signals, as well as signal processing algorithms to support the execution of the AAS features. Those are the combinations of many radios and their architectures [7]. The baseband unit of the AAS sends the signal to the antenna array for the final step of beamforming. Compared to conventional systems, AAS provides much greater flexibility and beamforming ability, in terms of adjusting the antenna radiation patterns to rapidly time-varying traffic and multi-path radio propagation conditions. In addition, multiple signals may be simultaneously received or transmitted with different beamforming patterns.

One of the important features of AAS is beamforming. Based on this technology, AAS can generate customized beams according to the information of UE position, so that the user can receive stronger signals. For the design of AAS, feature testing is one of the important tasks. The accuracy of beamforming pattern generation is an important requirement for AAS applications. In order to determine whether the result of specific beamforming is consistent with the expectation, a reliable and convenient beamforming test system needs to be proposed and established. The OTA or conducted test system in the laboratory can effectively help engineers verify the beamforming performance. There are many types of test instruments that can be used in the beamforming test system for simulating channel. One of them is the Butler matrix-based [8] beam simulation system.

Beam simulation system. In the beamforming test system, the Butler matrix-based beam simulation system is the core component that simulates the channel in different directions. With phase shifters and hybrid junctions, a beam simulation system can precisely add the fixed phase shift to the input signal. It usually works with a programmed attenuation system that can modulate the channel amplitude to realize the simple air interface simulation of the test channel between the BS and the UE. After connecting the test channel to the AAS and the UE simulator, this automatic test system can help

engineers evaluate the beamforming performance of AAS.

1.2 Motivations and Project Problem

As the core component of the beamforming test system, the beam simulation system needs to operate with high accuracy. Therefore, the verification of beam simulation system is an important prerequisite to ensure the precision of the beamforming test system. A test is needed to verify the reliability of the system and it is required to be time-efficient and accurate. An additional requirement is that the test needs to provide some information that can help engineers locate the faulty component within the circuit diagram when the system is verified to be faulty.

This thesis verifies a beam simulation system and summarizes the characteristics of this system. An innovative and efficient test method is used for assessing the beam simulation system. This method can identify the possible faulty parts of the system circuit by executing a simplified test scheme. One advantage of this method is that it can utilize the existing resources, i.e., CSI-RS signals as the reference signal for beamforming verification. In short, the validity of the beam simulation system is evaluated by CSI-RS signals simulation and measurement.

This thesis work have evaluated the validity of this beam simulation system. It includes the following steps [4].

1. A system that is built in the laboratory for realizing beamforming signal transmission test is investigated. The 5G physical layer protocol, especially the CSI-RS codebook standard is reviewed.

2. After the simulation, the theoretical performance of the device is derived. Based on the combination of different CSI-RS codebooks and beam simulation system, the theoretical received power for different directions can be derived by using the MATLAB simulation tool.

3. A series of measurements on this beamforming test system is conducted by using different configurations, specifically different precoding schemes, measurement result which collected from the spectrum analyzer is compare with the simulation result.

4. Based on the comparison study of the system performance, the conclusion is given whether the beam simulation system is working within the expected performance range.

In the actual environment, spectrum resources are scarce. Therefore, the lack of resources leads to an evolution of the current communication system. AAS has a hardware radio unit that comprises an antenna array, radio chains as well as parts of the baseband, and a multi-antenna feature (such as beamforming and MIMO) that can be executed in the AAS radio and baseband unit [9]. Compared with reciprocity-based beamforming which has a large amount of received data to be processed at the BS, codebook-based beamforming has great potential in the future development of beamforming technology [10] because it can effectively reduce the complexity and improve beamforming efficiency.

The development of technology can help us solve the lack of spectrum resources, so the evaluation of some technologies is also an important part of the development process. For beamforming verification, the RF network beamforming test system can simplify the field test to the lab test. It can save a lot of time and reduce the cost of testing compared with

traditional field tests. The beam simulation system is the core module of the beamforming test system. Therefore, validating the beam simulation system is an important prerequisite for implementing this beamforming test system. If the beam simulation system is faulty, the measurement results given by the system will not correspond to the real performance of the beamforming. Analysis based on these results is also untenable. Testing this beam simulation system can not only verify the correctness of the device but also give the exact deviation between the actual performance and theoretical performance of the beam simulation system. Afterward, technicians can perform beamforming verification more efficiently based on this assessment. At the same time, the innovative test scheme can also help engineers to reduce the iteration of tests to find the faulty parts of the circuit in a short time.

1.3 Outline of the Thesis

Each of the following chapters corresponds to a different topic.

Chapter 2 focuses on basic concepts and technology theory. Antenna array and MIMO system are firstly described. AAS is discussed in the second part of chapter 2.

Chapter 3 gives an overview of the beamforming test system, including the introduction of hardware blocks.

Chapter 4 describes the CSI-RS, the assessment methodology and procedure of simulation and actual measurement are also included.

Chapter 5 gives an interpretation to the simulation methodology and describes the simulation results for different CSI-RS precoding configurations.

Chapter 6 includes measurement results for different CSI-RS codebooks and a comparison study to give a comprehensive performance image of this beam simulation system.

In Chapter 7, the conclusions and future work are discussed.

2

Basic Concepts and Techniques

This chapter introduces primarily technical knowledge to help understand the measurement and simulation results. More detailed knowledge can be obtained by referring to relevant papers [11]. MIMO and beam simulation system based on Butler matrix are mainly described because the following chapters will focus on the analysis of these two techniques. As the technologies implemented and devices used in this project, the following definitions can help to understand the purpose of the assessment and assessment result.

2.1 Multi-beam Antenna

Multi-beam antenna is an antenna device that can generate multiple beams. It adds more features to the systems that it is a part of, boosts the capacity of communications systems, preserves the limited frequency spectrum and other limited assets, and reduces interference from environments. Based on these characteristics, the multi-beam antenna is the fundamental part of the MIMO system that requires flexibility. These beams can be combined into one or several shaped beams to cover a specific space. There are three basic types of multi-beam antennas, lens antenna, reflective antenna, and phased array. Compared with reflective multi-beam antenna and lens multi-beam antenna, which rely on optical beam generation principles, a phased array with multiple antennas is a more straightforward approach that can be integrated with the antennas on a single substrate.

A phased array antenna is a grid of antenna elements assembled, where the radiation pattern of each element is structurally combined with the radiation patterns of adjacent antennas to form an effective radiation pattern called the main lobe that radiates power to the desired direction. Another purpose of the phased array design is to create nulls and side lobes in the undesired directions. In short, the phased array is designed to maximize the power radiated to the main lobe while reducing the power radiated to the side lobes to acceptable levels.

Another critical aspect of phased array antenna design is the spacing of the antenna elements. Once the system goal has been determined by setting the number of elements, the physical array diameter is mainly determined by the size constraints of each element, which should be less than one-half wavelength to prevent grating lobes. Grating lobes radiate power in unwanted directions.

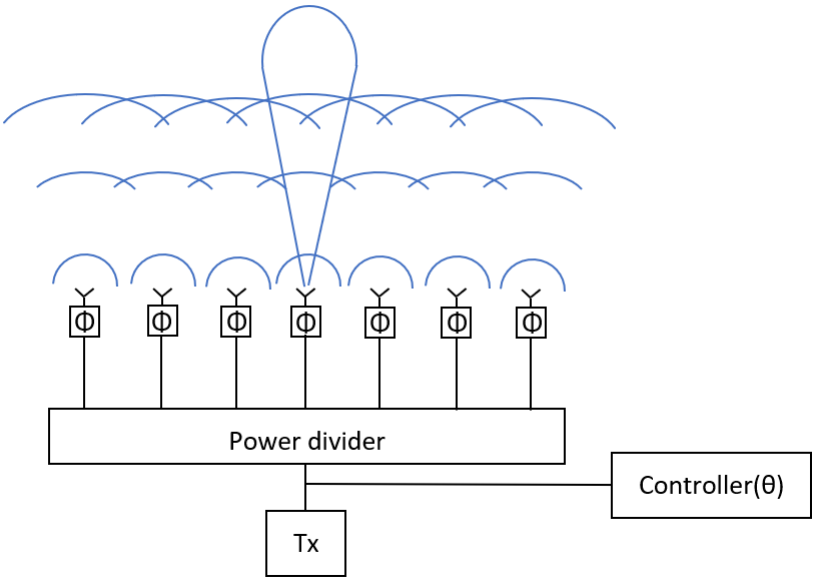

Figure 2.1: Phased array

2.2 Beamforming

Next-generation antenna technologies take advantage of the capacity provided by multi-beam antenna. The so-called beamforming is the technology that can achieve good performance in different environments by focusing radio power through the radio channel toward a specific receiver. With beamforming technology, the radio system can adjust its radiation pattern by processing the signal amplitude and phase and applying them to the antenna element. The beamforming-supported radio system consists of a signal controller and an array antenna, which realizes spatial steering by adjusting the signal amplitude and phase of the array elements. The benefits of beamforming are that it can realize large channel capacity, low power consumption, and strong anti-interference ability.

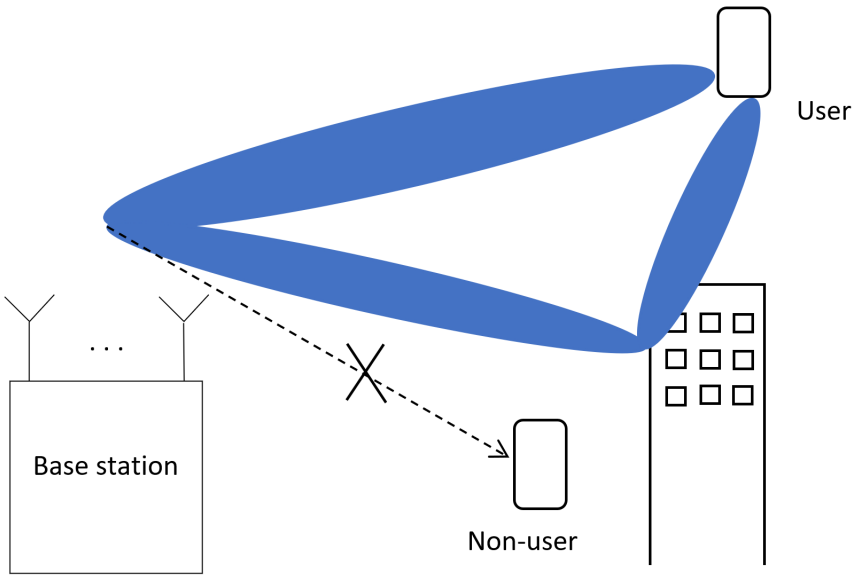

Figure 2.2: Generalized beamforming

In mobile communication implementations, the radio system like AAS uses an antenna array to generate a narrow beam with high gain in the direction of a user, while not generating a beam in the direction of a non-user. At the same time, beamforming can also help the receiver side to collect the signal power from a specific transmitter or direction. In addition, transmitting power in only one direction does not always show the optimum result. Many scenarios in real transmission are multi-path scenarios, where the radio channel comprises multiple propagation paths from the transmitter to receiver through diffraction around corners and reflections against large objects, it is beneficial to transmit the same signal in several different propagation paths with phases and amplitudes controlled in a way that they add constructively at the receiver. This is referred to as generalized beamforming, as shown in Fig. 2.2. As part of generalized beamforming, it is also possible to reduce interference signal to other UEs. This is achieved by controlling the transmitted signals to make them cancel each other out at the non-user.

2.3 MIMO

Conventional mobile communication systems use single-antenna transceivers so-called Single Input Single Output (SISO) system. In the SISO system, both the transmitter and receiver of the data stream are equipped with only one antenna. Compared with the SISO system, the MIMO system has significant advantages such as high transmission rate and stable transmission. Therefore, MIMO technology has been widely used in many modern wireless communication standards, especially in the consumer field. MIMO technology means that a data stream is transmitted into the channel by more than one antenna and received by more than one antenna when it leaves the channel. Multiple antennas at the transmitter and receiver introduce signal degrees of freedom that are not present in SISO systems. This refers to the spatial degrees of freedom of the signal which can be obtained by spatial multiplexing and spatial diversity. Overcome adverse effects in the wireless channel to achieve the goal of improving communication quality.

In the MIMO system, multi-path fading improves the spatial freedom of the wireless system. If the path gain fading between each transceiver antenna is relatively independent, a complex parallel spatial channel will be formed. Assuming that different data can be transmitted in sub-channels, the data transmission speed of the entire system can be greatly improved. This technology is called spatial multiplexing. Spatial multiplexing plays an important role in high signal-to-noise ratio regions in systems with limited degrees of freedom. The measure of its performance is the maximum capacity that the system can provide.

On the other hand, MIMO systems can also achieve spatial diversity to counteract channel fading. The MIMO system can ensure the reliability of wireless transmission by improving the diversity gain. The target of this technology is to provide multiple independent fading copies of data for the receiver to reduce the probability that all signals are affected by deep fading at the same time. For example, assuming that the received signals of the two receive antennas are interfered by noise, a signal of higher quality can be reconstructed by combining the two sets of received signals. Space diversity is mainly used to compensate for the randomness of channel fading. The most common examples of diversity include space-time coding and beamforming.

2.4 MIMO Communication

The MIMO system refers to a communication system using multiple antennas at the transmitter and receiver simultaneously, which effectively utilizes random fading and possible multi-path propagation to multiply the service transmission rate. Its core technology is space-time signal processing, that is, using the combination of multiple time and space domains distributed in space for signal processing.

MIMO channel is the intermediate process through which a signal is transmitted from a transmitter to a receiver. Between the transmitter and the receiver, there needs to be some kind of medium to transmit the signal, this medium can be a wired medium or wireless medium. This medium with attenuation and interference is called a channel. For deployed 5G base stations, signals are usually transmitted over a wireless medium. In our test system, the signal propagates through a wired medium. But the test equipment in the test system can simulate a real wireless channel. Consider a MIMO system in which the BS has M antennas and M_{RF} RF chains [12]. When the base station transmits the data stream to users, the number of users is U and served by M_S data streams. The uth user is equipped with N_u antenna elements and $N_{RF,u}$ RF chains, respectively, and $N_{S,u}$ data streams are applied for this user. The data symbol will firstly go through a baseband

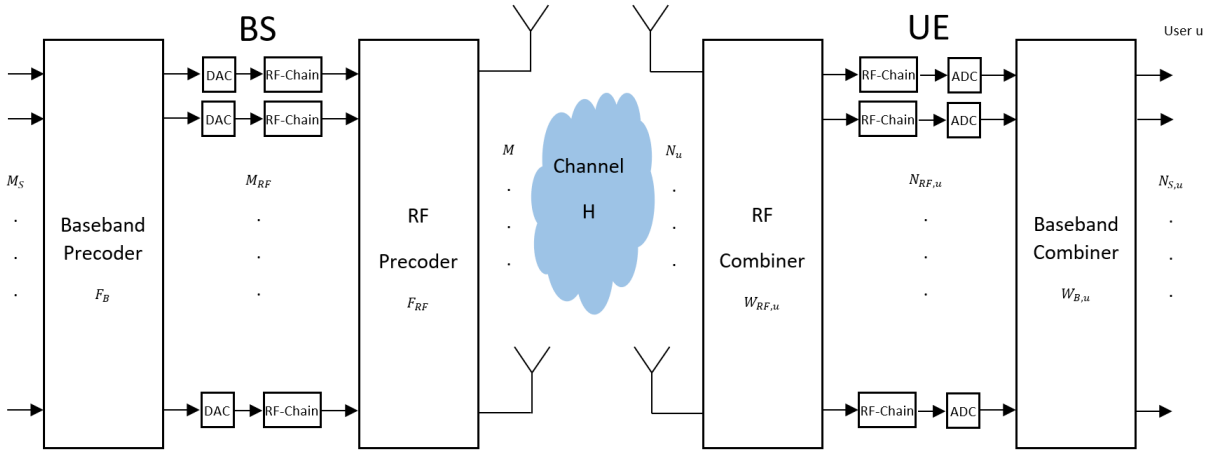

Figure 2.3: MIMO channel representation

precoder and then an RF precoder, which all have a matrix for precoding. Therefore, the transmitted signal S_T [13] is defined as

$$S_T = F_{RF} F_B S \tag{2.1}$$

For this equation, F_B and F_{RF} are the baseband digital precoding matrix and RF precoding matrix respectively. S is the symbol vector at the BS side. On the UE side, after the signal has passed through the channel, the received signal S_R at the antenna ports of UE is

$$S_R = H S_T + N \tag{2.2}$$

H is the MIMO channel transfer matrix and N is the white Gaussian noise. After the signal is received by UE, an RF combiner is firstly used to decode the received signal by RF combining matrix W_{RF}. Next, the received signals are combined in the baseband domain with the digital combining matrix W_B. Then the received data symbol Z_R is

$$Z_R = W_B W_{RF} H F_{RF} F_B S + W_B W_{RF} N \tag{2.3}$$

This is the processed data symbol in downlink transmission. The parameters of the symbol will be displayed on the spectrum analyzer. The adaptive W_{RF} and F_{RF} make reproducing

the MIMO channel matrix $W_{RF}HF_{RF}$ incapable, e.g., using the radiated two-stage method [14]. The feasible solution for hybrid massive MIMO should be reproducing H.

2.5 MIMO Channel and Antenna Array

The wireless propagation environment and the antenna radiation patterns of transmitter and receiver are factors that determine channel transfer matrix H. To derive a comprehensive geometrical channel model, the time-dependent dynamic channel should be involved with the complex polarimetric gains, angles, Doppler frequencies, propagation delays, and so on of multi-path components. For subcarrier f and time t, the $H(f,t)$ is

$$\begin{aligned} H(f,t) = &\sum_{l=1}^{L(t)} G_{Rx}(f,-k_l^{Rx}(t))A_l(f,t)G_{Tx}^T(f,k_l^{Tx}(t)) \\ &\times \exp\left\{j2\pi\int^t v_l(t')dt'\right\}\exp\left\{-j2\pi f\tau_l(t)\right\} \end{aligned} \tag{2.4}$$

$A_l(f,t)$ is the polarimetric amplitude matrix

$$A_l(f,t) = \begin{bmatrix} a_l^{aa}(f,t) & a_l^{ab}(f,t) \\ a_l^{ba}(f,t) & a_l^{bb}(f,t) \end{bmatrix} \tag{2.5}$$

where, τ_l and v_l stand for propagation delay and Doppler frequency for lth path, L is the number of paths, a and b stand for the polarization pair of the antenna at Tx and Rx, respectively. In addition, $k_l^{Tx/Rx}$ represents the wave vector in the departure or arrival direction at the Tx/Rx side for the lth path. The G_{Tx} and G_{Rx} are the polarimetric antenna pattern matrices for Tx and Rx.

MIMO channels are described in above. For the path with a specific angle, $G_{Rx}G_{Tx}$ can be represented by a $M \times N$ manifold matrix G (steering vector matrix).

$$G = \begin{bmatrix} g_1(\omega_0) & g_2(\omega_0) & g_2(\omega_0) & ... & g_N(\omega_0) \end{bmatrix} \tag{2.6}$$

This thesis mainly involves line array and planar array. In this subsection, two spatial array delay expressions are derived to calculate the corresponding steering vectors. The basic expression of the steering vector is

$$g_i(\omega_0) = \begin{bmatrix} e^{-j\omega_0\tau_{1i}} \\ e^{-j\omega_0\tau_{2i}} \\ ... \\ e^{-j\omega_0\tau_{Ni}} \end{bmatrix} \; i = 1,2,...,M \tag{2.7}$$

$\omega_0 = 2\pi f = 2\pi\frac{c}{\lambda}$, λ is wavelength and c is the speed of light. If the delay τ between the array elements is known, the steering vector for a specific array can be derived. The following part shows the calculation of steering vectors for two kinds of array.

1) Uniform Linear Array (ULA)

As shown in Fig. 2.4, there are l elements arranged linearly on the z-axis, and the distance between the two array elements is d. Take the leftmost array element as the origin. The direction angle θ is the angle between the received signal and the y-axis. The coordinate vector of l array elements is [0, d, 2d, ..., (l-1)d]. The assumption is that there is only one signal direction. According to the geometric principle, the time delay of the signal

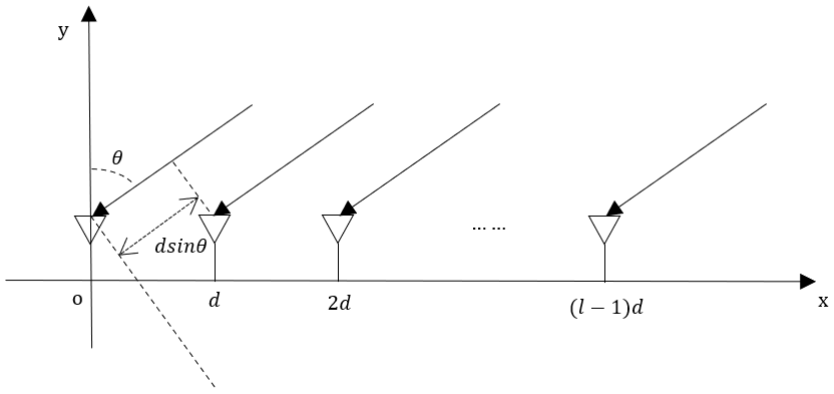

Figure 2.4: Uniform linear array

received by the second array element relative to the reference array element can be derived as

$$\tau_1 = \frac{d \sin\theta}{c} \tag{2.8}$$

c is the speed of light. Then

$$\varphi(\tau_1) = e^{-j\omega_0\tau_1} = e^{-j\omega_0 \frac{d\sin\theta}{c}} \tag{2.9}$$

Set $\omega_0 = 2\pi f = 2\pi\frac{c}{\lambda}$. Then

$$\varphi(\tau_1) = e^{-j2\pi \frac{c}{\lambda}\frac{d\sin\theta}{c}} = e^{-j2\pi \frac{d\sin\theta}{\lambda}} \tag{2.10}$$

Substitute the assumption $d = \lambda/2$ into the above equation, and simplify it

$$\varphi(\tau_1) = e^{-j\pi\sin\theta} \tag{2.11}$$

Extending the above derivation to the l array element, the relative delay of the received signal relative to the reference element is

$$\tau_1 = \frac{x_l \sin\theta}{c} = \frac{(l-1)d\sin\theta}{c} \tag{2.12}$$

Therefore, the signal received by the l element relative to the reference array element is

$$\varphi(\tau_1) = e^{-j(l-1)\pi\sin\theta} \tag{2.13}$$

From Equation 2.7 and Equation 2.13, it can be derived that the steering vector of the uniform linear array received signal for M elements is

$$\mathbf{g} = \begin{bmatrix} e^{-j\pi\sin\theta} \\ e^{-j2\pi\sin\theta} \\ \cdots \\ e^{-j(M-1)\pi\sin\theta} \end{bmatrix} \tag{2.14}$$

2) Planar Array (PA)

In Fig. 2.5, take the four-element array as an example. It is assumed that the signal only comes from a single direction. The distance between elements on an axis is d. Taking

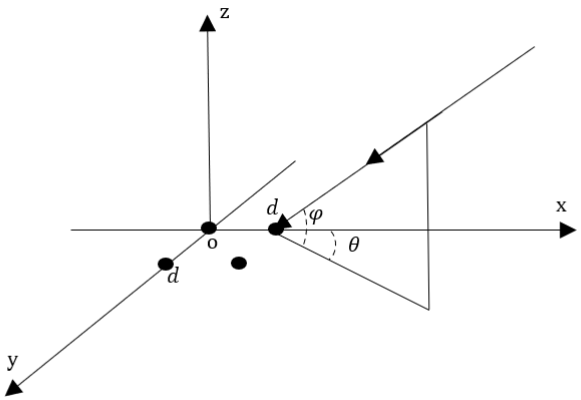

Figure 2.5: Planar array

the element at the origin as the reference element, the vector formed by the position components of each element in the x-axis direction is $\mathbf{x}_p = [0, 0, d, d]$. The vector formed by the position components of each array element in the y-axis direction is $\mathbf{y}_p = [0, d, 0, d]$. θ is the azimuth angle of the signal and φ is the elevation angle of the signal. The delay vector of each element relative to the reference element is

$$\tau = \frac{1}{c}(\mathbf{x}_p \cos\theta \cos\varphi + \mathbf{y}_p \sin\theta \cos\varphi) \tag{2.15}$$

Combining Equation 2.7 and Equation 2.16, the received signal of each element relative to the reference element is

$$\varphi(\tau) = e^{-j\omega_0\tau} = e^{-j\omega_0 \frac{1}{c}(\mathbf{x}_p \cos\theta \cos\varphi + \mathbf{y}_p \sin\theta \cos\varphi)} \tag{2.16}$$

when $\omega_0 = 2\pi f = 2\pi\frac{c}{\lambda}$ (f is carrier frequency) and $d = \frac{\lambda}{2}$, the steering vector of the received signal is

$$\mathbf{g} = \begin{bmatrix} 1 \\ e^{-j\pi \sin\theta \cos\varphi} \\ e^{-j\pi \cos\theta \cos\varphi} \\ e^{-j\pi(\sin\theta \cos\varphi + \cos\theta \cos\varphi)} \end{bmatrix} \tag{2.17}$$

The above derivation connects the steering vector to the signal angle. In the following content, the calculation of beamforming gain at a specific location is based on this theoretical derivation.

2.6 Multiple Antenna System

For network services, linear arrays and planar arrays are widely used because the structural characteristics of these two arrays are conducive to the directional coverage of the BS. The radio unit and antenna array in the conventional base station system are separated. With the development of 5G, the number of antennas is increasing, and there are more feeder interfaces on the radio unit, and the complexity of the process is getting higher and higher. In addition, the feeder cable itself has attenuation, which also affects the system performance. For this reason, in 5G, the radio unit and passive antenna array are integrated into one device, resulting in a compact multiple antenna system. AAS is an outstanding development example that successfully integrates multi-antenna technology and antenna arrays in a relatively small device.

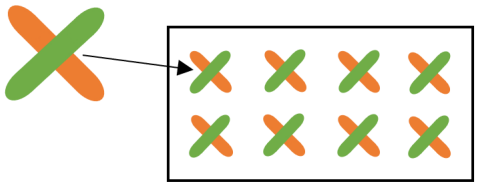

Figure 2.6: A typical antenna array is made up of individual dual-polarized antenna elements

AAS is the recent technology developments that have made AAS a viable option for large-scale deployments in existing 4G and future 5G mobile networks [15]. AAS enables the latest beamforming and MIMO techniques that are advanced tools for improving the quality of service, capacity, and signal coverage. As a consequence, AAS significantly boosts wireless communication performance in both uplink and downlink.

Nowadays, the methods to realize the miniaturization of AAS include reducing the number of elements, reducing the element spacing, and dual-polarization design. While keeping the element spacing constant, reducing the number of elements usually results in a decrease in array gain. Reducing the element spacing will also lead to this undesired result because the coupling between the elements will become severe.

In order to further improve the miniaturization design of AAS, the orthogonal dual-polarization design of array elements is widely adopted (Fig. 2.6). Using dual-polarization array elements instead of single-polarization array elements reduces the number of array elements by half while the number of ports remains the same. As a result, the size of the array is decreased. Dual-polarization array elements can utilize polarization diversity to achieve the same result as space diversity antennas. Because the two polarization directions are orthogonal, the signals sent out have irrelevant fading characteristics, which in turn realize polarization diversity.

AAS usually uses $\pm 45^{\circ}$ dual-polarized array elements. Therefore, using a dual-polarized array allows the system to realize polarization diversity receiving technology, and the diversity gain effectively compensates for the array gain loss caused by the reduction of the array antenna aperture.

3

Lab Test System

This chapter primarily gives a detailed description of the beamforming test system, which includes the BS part, the channel part, and the mobile station part. Usually, the purpose of this system is to assess the validity of the base station. In this thesis, the beam simulation system under test is the module within the channel part.

3.1 Structure of Testing System

The conventional field test has been proven to be the most accurate MIMO measurement method. However, the field test is time-consuming and difficult to implement. A test often takes engineers a lot of time to draw up and implement a detailed test plan. The development of test equipment has made it possible to conduct MIMO testing in the laboratory and successfully convert field testing to laboratory testing. Compared to field testing, the characteristic of laboratory testing is that it uses channel simulation equipment to simulate the real channel. In the testing process, the theoretical results of the received signal are simulated first and then compared with the actual test results to verify the performance of the MIMO system. Fig. 3.1 shows the basic framework of the test system.

The diagram of the beamforming test system is shown in Fig. 3.2. The base station consists of a baseband unit, radio with antenna array, and beam simulation system. For the specific description of applied devices, the beamforming test system consists of a baseband unit controlled by MOSHELL which is a Linux-based bash shell, and a radio (with 4x8 sub-arrays) works with the baseband unit to generate the signal and then fed it into the beam simulation system for direction simulation. The 8 output RF chains are processed by the Cellular Coaxial Network (CCN) and received by the UE. CCN is an RF switch that can control which output will be observed and add attenuation. During the study, different CSI-RS codebook configurations for the radio system are implemented. These operations are performed remotely on the device through the Citrix workspace.

The channel scenario that the test system can simulate is the Line-of-Sight channel. In addition, the system supports single-user and multi-user MIMO testing. In this thesis, the assessment of beam simulation system is conducted in the single-user scenario.

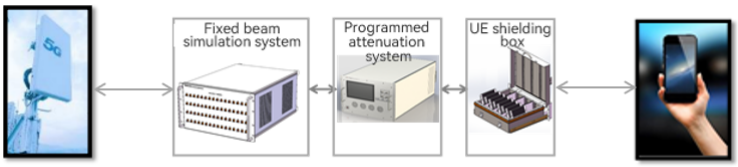

Figure 3.1: Beamforming test system

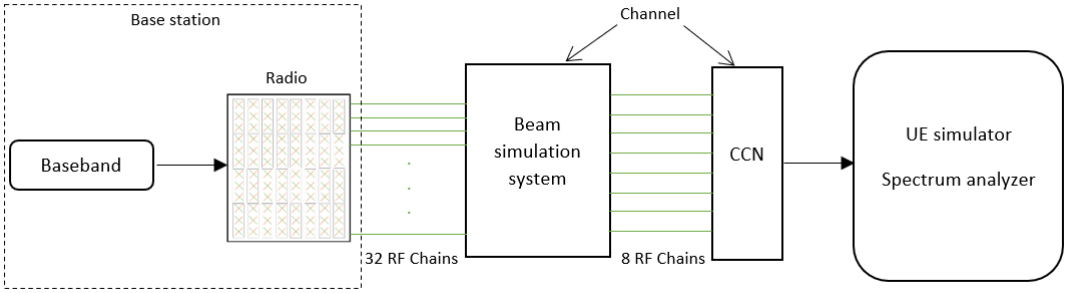

Figure 3.2: Diagram of the beamforming test system built in lab

3.2 Butler Matrix and Beam Simulation System

The beamforming circuit enables the integration of antenna arrays onto a substrate. The phase shifter and the coupler are connected to form a feed network through the microstrip, so as to realize the phase distribution [16]. Due to the dispersion of the beamforming network, the angle of the beam and its associated beamwidth will vary with frequency. Various beamforming circuits have been proposed and studied, the most typical of which is the Butler matrix [17] and the Blass matrix [18].

The circuit shown in Fig. 3.3 is a typical 4×4 Butler matrix structure consisting of two cross-couplers, two $-45°$ phase shifters, and four 3 dB bridges. It has four input ports and four antenna ports. After each component in the Butler matrix performs power division and phase shift operations on the input signal, four-phase distributions can be achieved at the four output ports to generate four beams pointed at different angles. When the signal is input from P1, the signal amplitude and phase at the output port can be derived as

$$A1 = \frac{1}{4}P1\angle 135° \tag{3.1}$$

$$A2 = \frac{1}{4}P1\angle 90° \tag{3.2}$$

$$A3 = \frac{1}{4}P1\angle 45° \tag{3.3}$$

$$A4 = \frac{1}{4}P1 \tag{3.4}$$

From the equation, it can be seen that the output power of each antenna is a quarter of the total input power, and the phase difference of the output ports is $-45°$. On the other hand, when the input ports are P2, P3, and P4 respectively, the phase difference of corresponding output ports is shown in Table 3.1.

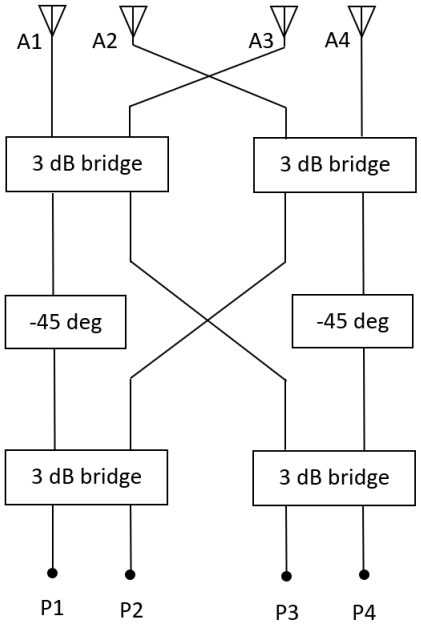

Figure 3.3: Structure of 4×4 Butler matrix

Table 3.1: Phase difference corresponding to different ports

Input port	Phase difference between adjacent output ports
P1	$-45°$
P2	$135°$
P3	$-135°$
P4	$45°$

With the help of the Butler matrix structure, a fixed beam simulation system is designed to apply the phase shift to the input signal and then achieve directional simulation at the output port. The fixed beam simulation system is a test device applied between the BS and mobile terminal. It is a multi-input multi-output matrix network, which can form multiple beams through a fixed beam matrix using an antenna beamforming network composed of hybrid joints and fixed phase shifters. The beam simulation system is suitable for multiple frequency bands and has a variety of input and output configurations, such as 32 inputs and 8 outputs, 32 inputs and 16 outputs, etc. This system efficiently reduces the complexity of BS testing and saves a lot of time compared to traditional field testing.

Based on this beam simulation system, the received signal power of the UE in several different directions can be simulated. In our system, the received signal power is measured at 8 locations.

3.3 Structure of Antenna Array

Usually, the test object of this test system is AAS, but in this paper, the test object is beam simulation system. Therefore, the AAS is a part of test system and is considered flawless. There are normally 16 or 32 antenna sub-arrays in the AAS we usually design. The sub-array may involve 2 to 4 cross-polarized antennas, all with two connections, one for each antenna polarization. Each sub-array is connected to one Transmitter (Tx) and

one Receiver (Rx) branch per antenna polarization so in total there are 32 or 64 receiver branches and 32 or 64 transmitter branches in the AAS. The sub-array works as one antenna but with a larger area for better antenna gain. The AAS in our test system has 32 sub-arrays and each sub-array consists of 3 cross-polarized antennas. This AAS is calibrated and verified. See below Fig. 3.4.

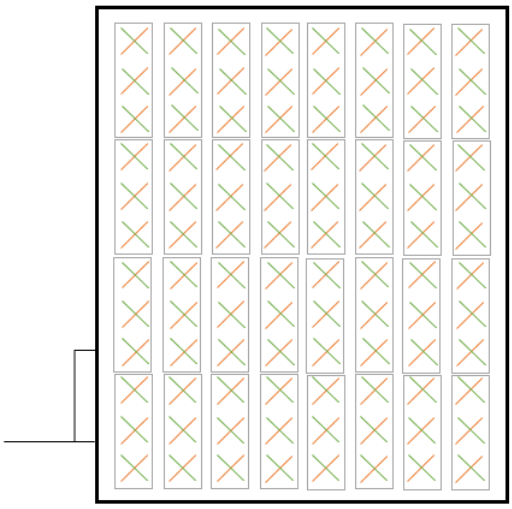

Figure 3.4: Antenna arrays with 4×8 sub-arrays

In real applications and field testing, the cross-polarized antennas transmit signals at the same time. In our test system, however, two polarization (polarization 0 and polarization 1) were connected to two beam simulation systems via cables respectively. That is the reason why there are only 32 RF chains instead of 64. The beam simulation system we assessed was connected to the antenna with polarization 0. Some of the parameters of this AAS are in Table 3.2

Table 3.2: AAS product description

Frequency range	2496 to 2690 MHz
NR tilt range	-3 to 11 degrees
Antenna	64Tx 64Rx
Sub-array	3

The antenna system operates at frequencies of 2496 - 2690 MHz and supports digital tilt -3 to 11 degrees.

3.4 Interpretation of Beam Simulation System

Based on the Butler matrix architecture, the beam simulation system can help demonstrate the beamforming performance of the antenna system with cost efficiency. The output port of the antenna system is connected to the input port of the beam simulation system with cables. With hybrid junctions and fixed phase shifters, the beam simulation system can adjust the signal phase of each input port and combine them at the output port to simulate the signal power of the antenna for multiple directions. For example, if we consider a simple beam simulation system (Fig. 3.5) with 4 input and 4 output ports. The physical angle of each output port is determined by the frequency. The signal power in the B4 direction can be measured if the A1 signal has 90 degrees phase shift before A0, the A2 signal has

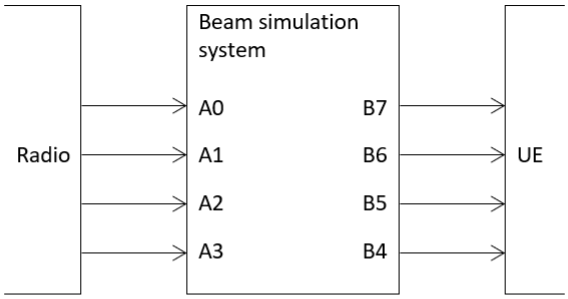

	A0	A1	A2	A3
B4	1	-i	-1	i
B5	1	1	1	1
B6	-i	1	i	-1
B7	1	-1	1	-1

1 means 0 degree phase shift

i means 90 degrees phase shift

-1 means 180 degrees phase shift

-i means 270 degrees phase shift

Figure 3.5: Simple beam simulation system for vertical direction

90 degrees phase shift before A1, A3 signal has 90 degrees phase shift before A2. As illustrated in Fig. 3.6, the distance between the center of A0 and the center of A1 is δ. Then the gap of propagation distance between A0 and A1 is $d = \delta \times \sin(\theta)$. For our system, the carrier frequency is 2625 MHz and then the wavelength is 11.4 cm. The 90 degrees phase shift corresponds to a quarter of the wavelength, so the d is around 2.85 cm. If δ is 3×0.058 m (because AAS has 3 sub-arrays in the column), then the physical angle of B4 = -9.30 degrees can be derived by

$$\theta = \arcsin \frac{d}{\delta} \tag{3.5}$$

The 180 degrees phase shift corresponds to half of the wavelength, so the delay is around 5.7 cm. If the delta is 3×0.058 m (because AAS has 3 sub-array in the column), then the physical angle of B7 = 19.12 degrees. The real beam simulation system has 32 input ports and 16 output ports. In this thesis, only 8 out of 16 output ports are measured. B1 (Left), B2 (Up Left), B4 (Down), B5 (Boresight), B6 (Up), B9 (Right), B10 (Up Right), B13 (Very Left/Right). Table 3.3 shows the phase shift added to different input ports. The validity of this beam simulation system can be effectively assessed by measuring the results of these eight ports. The numbering scheme between the AAS antenna element and the input port of the beam simulation system is shown in Fig. 3.7. Because each output port of the beam simulation system represents a simulated channel, the accuracy of the beam simulation system has a critical impact on the AAS testing. If the beam simulation system has a large error, the simulated channel will not match the real channel, causing engineers to give a wrong assessment of the AAS performance. Therefore, the beam simulation system needs to be tested and calibrated before this test system is put into use.

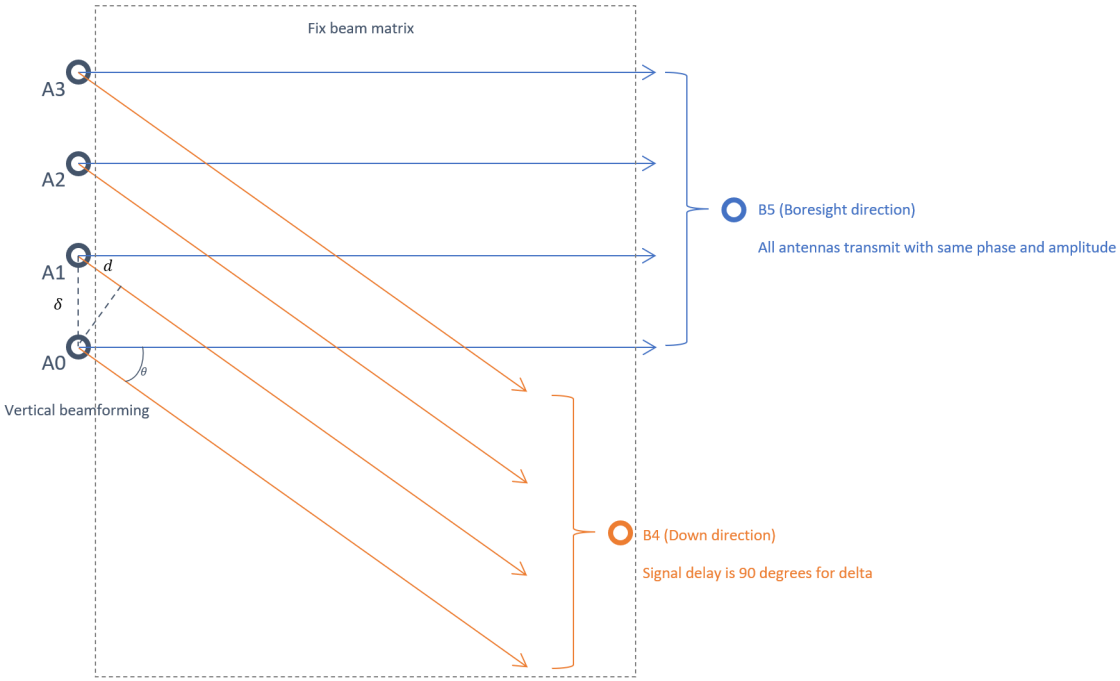

Figure 3.6: Physical angle interpretation for vertical direction

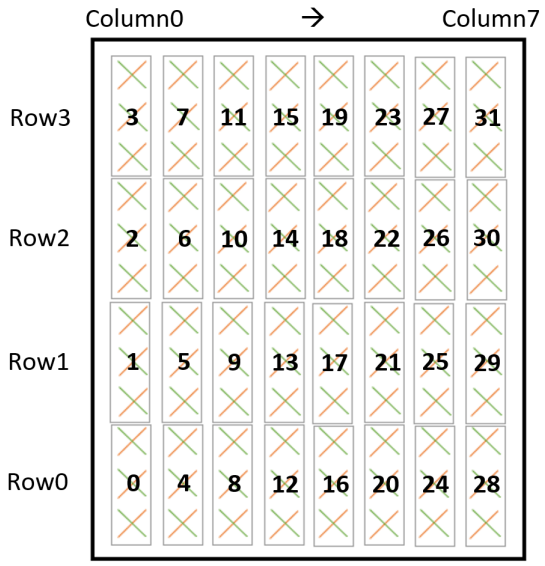

Figure 3.7: AAS antenna elements numbering scheme

Table 3.3: Beam simulation system description

Output port / Antenna element	B1	B2	B4	B5	B6	B9	B10	B13
A0	1	-i	1	1	-i	-i	-1	1
A4	-i	-1	1	1	-i	1	-i	-1
A8	-1	i	1	1	-i	i	1	1
A12	i	1	1	1	-i	-1	i	-1
A1	1	1	-i	1	1	-i	-i	1
A5	-i	-i	-i	1	1	1	1	-1
A9	-1	-1	-i	1	1	i	i	1
A13	i	i	-i	1	1	-1	-1	-1
A2	1	i	-1	1	i	-i	1	1
A6	-i	1	-1	1	i	1	i	-1
A10	-1	-i	-1	1	i	i	-1	1
A14	i	-1	-1	1	i	-1	-i	-1
A3	1	-1	i	1	-1	-1	i	1
A7	-i	i	i	1	-1	1	-1	-1
A11	-1	1	i	1	-1	i	-i	1
A15	i	-i	i	1	-1	-1	1	-1
A16	1	-i	1	1	-i	-i	-1	1
A20	-i	-1	1	1	-i	1	-i	-1
A24	-1	i	1	1	-i	i	1	1
A28	i	1	1	1	-i	-1	i	-1
A17	1	1	-i	1	1	-i	-i	1
A21	-i	-i	-i	1	1	1	1	-1
A25	-1	-1	-i	1	1	i	i	1
A29	i	i	-i	1	1	-1	-1	-1
A18	1	i	-1	1	i	-i	1	1
A22	-i	1	-1	1	i	1	i	-1
A26	-1	-i	-1	1	i	i	-1	1
A30	i	-1	-1	1	i	-1	-i	-1
A19	1	-1	i	1	-1	-1	i	1
A23	-i	i	i	1	-1	1	-1	-1
A27	-1	1	i	1	-1	i	-i	1
A31	i	-i	i	1	-1	-1	1	-1

4

Methodology for Calibrating the Beam Simulation System

This chapter gives an interpretation of CSI-RS which is the test signal, and method of beam simulation system assessment. Because each antenna port of the CSI-RS will be transmitted by different sets of antenna elements, the input ports of the beam simulation system can be divided into several groups for testing based on this characteristic. With the help of CSI-RS, the time required for assessment is effectively reduced.

4.1 Channel State Information Reference Signal

Current radio access technologies can utilize channel information to optimize radio transmission. The specific implementation method is that the base station transmits the reference signal, and optimizes the subsequent downlink based on the acquired channel information. This observation process is called "Channel Sounding". It requires that the receiver can measure the channel characteristics of a specific reference signal. There are two kinds of support for channel sounding in NR. Downlink CSI-RS and uplink Sounding Reference Signals (SRS). This thesis presents a new exploration of the use of CSI-RS by evaluating the beam simulation system based on CSI-RS signal measurement.

4.1.1 CSI-RS Structure

The reason for introducing CSI-RS [19] is the extension of Long-Term Evolution (LTE) to support spatial multiplexing with more than four layers. CSI-RS is considered valuable in NR and is further extended to a more detailed channel sounding. For example, to provide support for beam management and mobility as a complement to the synchronization signal block (SSB).

Each port in CSI-RS represents a sounding channel and can support up to 32 ports. CSI-RS is configured individually for different antenna devices. But this does not mean that the transmitted CSI-RS is only used by a single device. CSI-RS is shared among devices in real-world scenarios.
As illustrated in Fig. 4.1, a single resource element within a block corresponds to one resource block in the frequency domain and one slot in the time domain is occupied by a single port of the CSI-RS. Regarding the location of CSI-RS, there are some restrictions to avoid collision with other downlink signals. For example, configured control resource set signals, SSB, and demodulation reference signals associated with Physical Downlink Shared Channel (PDSCH) transmissions scheduled for the device. For multi-port CSI-RS, a set of resource elements is transmitted orthogonally. This transmission is based on the

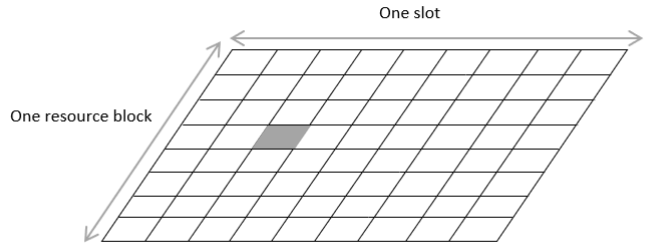

Figure 4.1: A single resource element within a slot/resource block for one port CSI-RS

integration of

Time-Domain Sharing (TDM). Different CSI-RS for each antenna port are transmitted in different OFDM symbols within a slot.

Frequency-Domain Sharing (FDM). Different CSI-RS for each antenna port are transmitted on different subcarriers within an OFDM symbol.

Code-Domain Sharing (CDM). Different CSI-RS for each antenna port are transmitted on the same set of resource elements with different orthogonal modulations.

Regarding CDM, for different scenarios, different CDM structures can be implemented for CSI-RS of antenna ports.

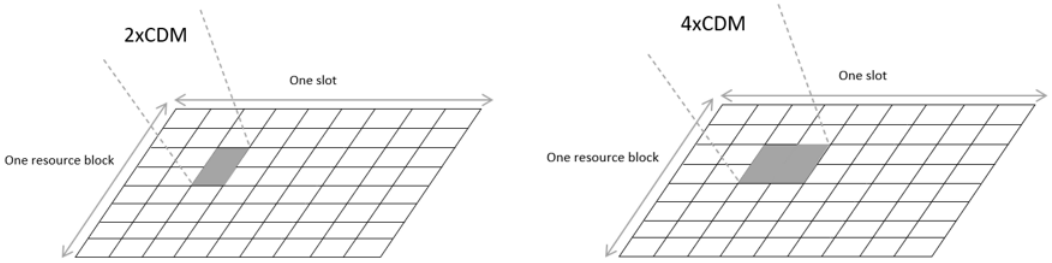

Figure 4.2: 2×CDM and 4×CDM structures for multi-port CSI-RS

As shown in Fig. 4.2, for 2×CDM, CDM is implemented on adjacent subcarriers, which means that code domain sharing is achieved between two CSI-RS ports. For 4×CDM, the time domain is also involved. CDM on two adjacent subcarriers and two adjacent OFDM symbols realizes code domain sharing between four CSI-RS ports.

As illustrated in Fig. 4.3, a two-port CSI-RS consists of two adjacent subcarrier resources in the frequency domain, which are shared by using CDM. The different CDM structures can be combined with FDM and TDM to configure different multi-ports CSI-RS structures. For the case where the CSI-RS corresponds to more than two antenna ports, the port configuration has flexibility. For a given number of ports, there are various CSI-RS structures based on different combinations of CDM, TDM, and FDM. As an example, there are two different structures for a sixteen-port CSI-RS, see Fig. 4.4.

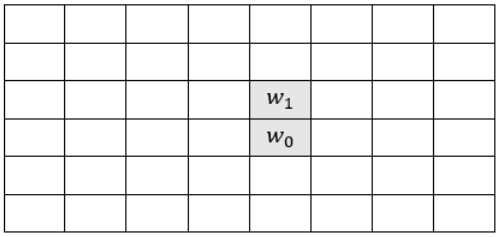

	w_0	w_1
Port 1	+1	+1
Port 2	+1	-1

Figure 4.3: Two ports CSI-RS based on 2×CDM and the orthogonal patterns of each port

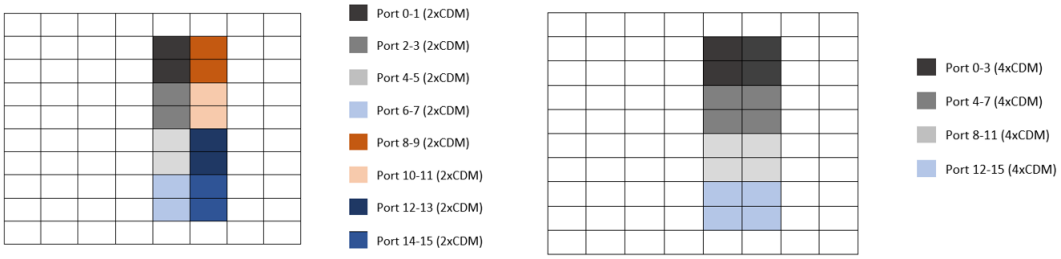

Figure 4.4: Two structures for 16 ports CSI-RS

The left part of the figure shows frequency-domain CDM over two resource elements (2×CDM) in combination with frequency and time multiplexing. The overall CSI-RS resource thus consists of eight subcarriers within two OFDM symbols. The right part of the figure shows time and frequency-domain CDM over four resource elements (4×CDM) in combination with frequency and two-time multiplexing. The overall CSI-RS resource thus consists of eight subcarriers within two OFDM symbols.

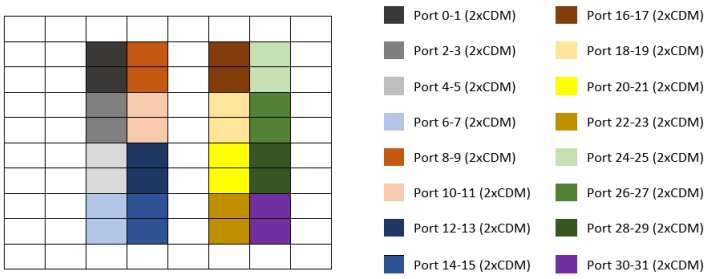

Figure 4.5: One structure for 32 ports CSI-RS

The maximum number of ports supported by CSI-RS is 32. Fig. 4.5 shows one of three 32-port CSI-RS configurations. This example shows that separate CSI-RS ports do not necessarily occupy consecutive OFDM symbols. In addition, separate CSI-RS ports do not necessarily occupy consecutive subcarriers. For multi-port CSI-RS, the correlation between CSI-RS and port number is first realized by CDM. Then FDM, and finally TDM. As shown in the 16-port example of Fig. 4.4, CDM separates the CSI-RS ports for consecutive port numbers. In addition, for the case of the right part, ports 0 to 3 are transmitted within one OFDM symbol, and ports 4 to 7 are transmitted within another OFDM symbol. These two sets of ports are separated by means of TDM.

4.1.2 CSI-RS Structure in Frequency Domain

The configuration of CSI-RS in the frequency domain is flexible. For a given bandwidth range, the CSI-RS can be configured to cover the full bandwidth or just cover a part of the bandwidth. For the case that the CSI-RS only covers a part of the bandwidth, the CSI-RS bandwidth and the starting position of the frequency domain are included in the configuration as parameters. Within a given CSI-RS bandwidth, the CSI-RS density is equal to 1 if the CSI-RS is configured to be transmitted on each resource block. If the CSI-RS is configured to be transmitted on every second resource block, the CSI-RS density is equal to 1/2. For 4-port, 8-port, and 12-port CSI-RS configurations, the 1/2 CSI-RS density is not supported. Meanwhile, the information about the set of resource blocks to which the CSI-RS will be transmitted should be included as the part of CSI-RS configuration for 1/2 CSI-RS density.

4.1.3 CSI-RS Resource Set in Time Domain

The CSI-RS structure also has multiple configurations in the time domain to provide flexibility. There are three configurations to define the transmission characteristics of the CSI-RS resource set, namely, periodic, semi-periodic, and aperiodic.

For periodic transmission, the CSI-RS is transmitted according to a predefined period N. The minimum number of N is 4 and the maximum number of N is 640. That is, the CSI-RS transmission occurs every N slot. In addition, the offset is also defined for periodic transmission to adjust the slot location of CSI-RS.

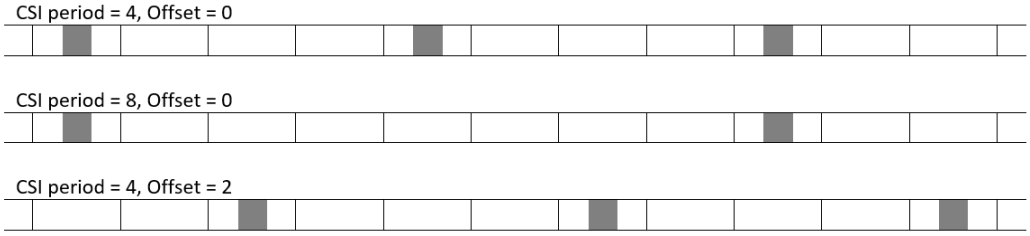

Figure 4.6: Examples of periodic CSI-RS and slot offset

For semi-periodic transmission, the periodicity of CSI-RS and slot offset are configured in the same way as for periodic transmission. The difference between periodic and semi-periodic transmission is that the latter has a switch mechanism called Media Access Control Control Elements (MAC-CE). When the transmission is activated, the CSI-RS signal will be transmitted according to the configured period and slot offset. When the transmission is deactivated, there will be no CSI-RS transmission until it is activated again. For aperiodic transmission, the device instantly knows the CSI-RS transmission by receiving a signal within the Downlink Control Indicator (DCI).

The periodic transmission is implemented for our test system, the CSI-RS periodicity is 40 slots. It needs to be clear that this periodicity is not a property of CSI-RS itself, but the property of the CSI-RS resource set.

4.1.4 Physical Antenna Mapping of CSI-RS

Multi-port CSI-RS corresponds to a set of antenna ports, and each antenna port is mapped to a set of antenna elements. However, antenna ports are usually not directly mapped

to a single physical antenna. In fact, the number of physical antennas to which CSI-RS is mapped is often larger than the number of antenna ports. Because for smart antenna, there will be multiple physical antennas on one antenna port. Sometimes an antenna element can be mapped on multiple antenna ports. For the CSI-RS codebooks used in this thesis, one antenna element will only be mapped to one antenna port. Fig. 4.7 shows how antenna elements are assigned to antenna ports of CSI-RS by a simple antenna array.

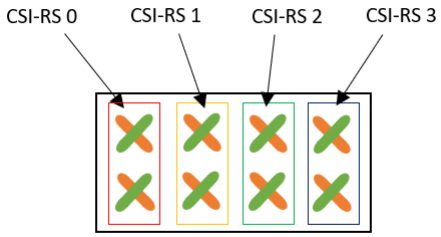

Figure 4.7: Example of physical antenna mapping of CSI-RS

When a UE executes channel sounding based on CSI-RS, the signal received by the UE will be M channel information corresponding to the M antenna ports. The power of the signal depends on the beam of each CSI-RS in direction of UE. Different antenna ports generate beams in different directions, and this difference is usually due to different precoding matrices. As illustrated in Fig. 4.8, the device can measure CSI-RS and report the recommended precoder matrix to the BS. The BS may then use the recommended precoding matrix for antenna mapping and weight implementation.

4.1.5 Precoder Matrix Mapping

Firstly, the CSI-RS signal transmits all precoding matrices (antenna port) for beam scanning. The recommended precoding matrix is then used according to the CSI report from the UE. The precoding matrix contains the information that which antenna elements are used and the weights for each antenna element. The weight is a complex vector with amplitude and phase that determines the signal fed to antenna elements.

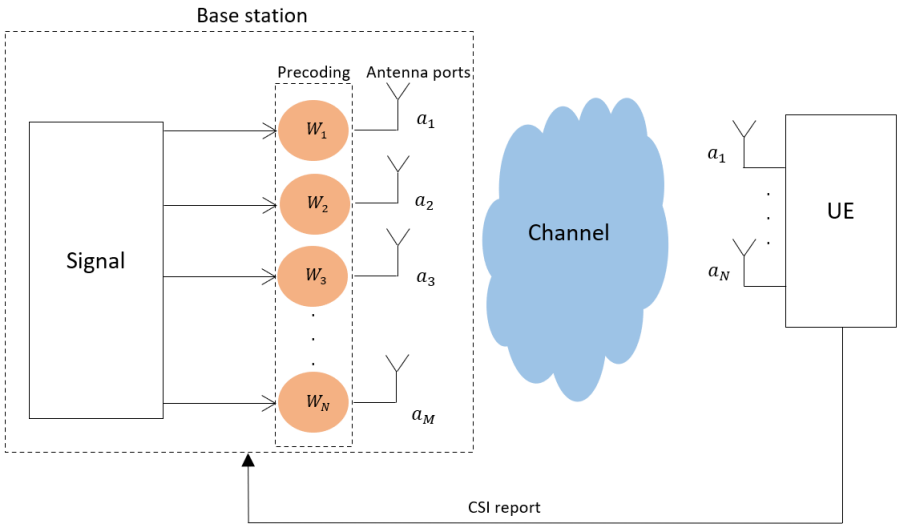

Figure 4.8: Precoding using CSI report

For our radio system, the combination of these precoding matrices is called W_{p2a}. Accord-

ing to the W_{p2a} matrix, the activated antenna ports and corresponding antenna weights for different antenna elements can be determined. For an antenna system, there are multiple W_{p2a} matrices to be implemented according to the scenarios and the number of antenna ports. For example, for the codebook with 8 antenna ports, the corresponding W_{p2a} also involves 8 antenna ports. For different deployment scenarios of the BS, there are corresponding optimized W_{p2a} matrices for CSI-RS beamforming. CSI reporting is not discussed in this thesis because the point of this thesis is the CSI-RS signal transmitted by the BS. The CSI-RS signal is fed to the input port of the beam simulation system through the coaxial cable.

4.2 CSI-RS Simulation and Measurement

CSI-RS signal is usually used to realize beamforming in wireless transmission. In this thesis, the CSI-RS signal is used as a tool to verify the validity of the beam simulation system. Because each antenna port of CSI-RS corresponds to a specific part of the antenna elements, the corresponding beamforming system input ports can be isolated for testing. If a large deviation between the simulation and measurement results of an antenna port is observed, it means that the problem originates from the components involved in these ports. The codebook of CSI-RS is the grid of all antenna ports used for channel sounding. For a specific codebook, the sounding signal transmitted from each antenna port can be extracted and measured individually. This is the fundamental principle of why CSI-RS can be used to isolate the beam simulation system input port for testing, since each antenna port corresponds to a group of input ports. For different codebooks, the group of beam simulation system input ports corresponding to each antenna port will also be different. Testing multiple codebooks can help us find the source of the failure more accurately. Meanwhile, the selection of the codebook will greatly affect the test efficiency and accuracy. Therefore, there should be certain differences between the selected codebooks, but they cannot be fully unrelated. In the thesis, the selected codebooks are given in Table 4.1. For instance, the CSI-RS 0 of 8 ports (4,1) codebook is transmitted by the antenna elements 0, 1, 4, and 5. The CSI-RS 15 of 16 ports (4,2) codebook is transmitted by the antenna elements 15 and 16.

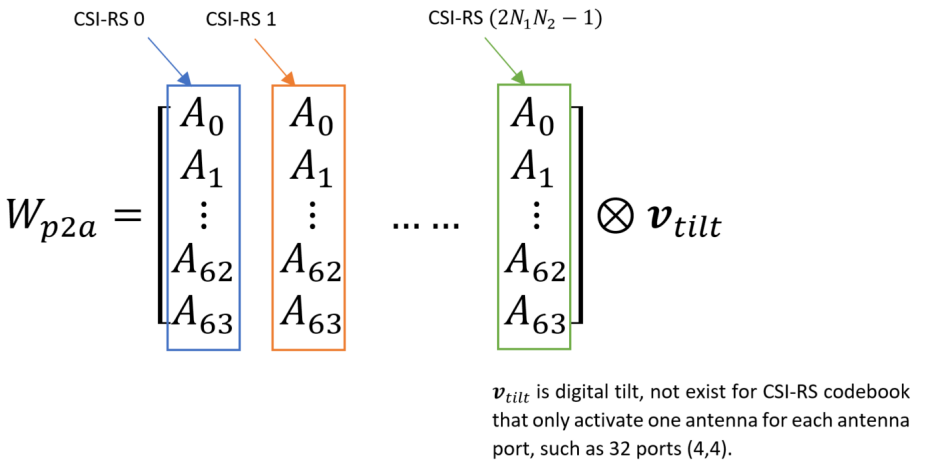

Figure 4.9: W_{p2a} matrix

8 ports (4,1), 8 ports (2,2), 16 ports (4,2), and 32 ports (4,4) codebooks are selected

Table 4.1: Selected CSI-RS configurations

CSI-RS ports	(N_1, N_2)	Port visualization
8	(2,2)	1 1 3 3 5 5 7 7 1 1 3 3 5 5 7 7 0 0 2 2 4 4 6 6 0 0 2 2 4 4 6 6
8	(4,1)	0 1 2 3 4 5 6 7 0 1 2 3 4 5 6 7 0 1 2 3 4 5 6 7 0 1 2 3 4 5 6 7
16	(4,2)	1 3 5 7 9 11 13 15 1 3 5 7 9 11 13 15 0 2 4 6 8 10 12 14 0 2 4 6 8 10 12 14
32	(4,4)	3 7 11 15 19 23 27 31 2 6 10 14 18 22 26 30 1 5 9 13 17 21 25 29 0 4 8 12 16 20 24 28

for comprehensive testing. The number of antenna ports can be derived by

$$P_{CSI-RS} = 2N_1N_2 \tag{4.1}$$

where 2 corresponds to two polarization, N_1 is the size of the horizontal dimension and N_2 is the size of the vertical dimension. The weight allocation of each antenna port is determined by the W_{p2a} matrix. For the W_{p2a} matrix, one column corresponds to one antenna port, and one row corresponds to one antenna element. Therefore, for different codebooks, the size of the W_{p2a} matrix is also different. For example, the W_{p2a} matrix of the 8 ports CSI-RS codebook consists of 8 columns and 64 rows. The W_{p2a} matrix of the 16 ports CSI-RS codebook consists of 16 columns and 64 rows. The reason why there are 64 rows in the matrix is that antennas for two polarization are included in W_{p2a}. Only the first 32 rows are considered since the beam simulation system connects with the antenna elements in Pol0. θ_{tilt} is the angle of digital tilt which is fixed at 3 degrees in this thesis.

Regarding the methodology for the assessment of the beam simulation system, measurements of CSI-RS signals were conducted for different CSI-RS codebooks in this thesis, and the gap between the B5 port (boresight) and other output ports was calculated. Then the theoretical received powers were derived by simulation. If there is an unacceptable deviation between the measured signal power and the simulated signal power, it means that the beam simulation system is not working as expected. At the same time, CSI-RS successfully isolates the input ports of the beam simulation system into several sets according to the codebook and then the combination of input and output ports corresponding to this CSI-RS signal can be identified.

5

Simulation Results

This chapter shows the steps involved in the simulation part using MATLAB and gives the simulation results. The 8 ports (4,1) codebook, 8 ports (2,2) codebook, 16 ports (4,2) codebook, and 32 ports (4,4) codebook were simulated in this thesis.

5.1 Steps of MATLAB Simulation

Step 1: Calculate the W_{p2a} matrix for selected CSI-RS codebooks. For example, the W_{p2a} matrix of 8 ports (4,1) codebook is given in Fig. 4.1.

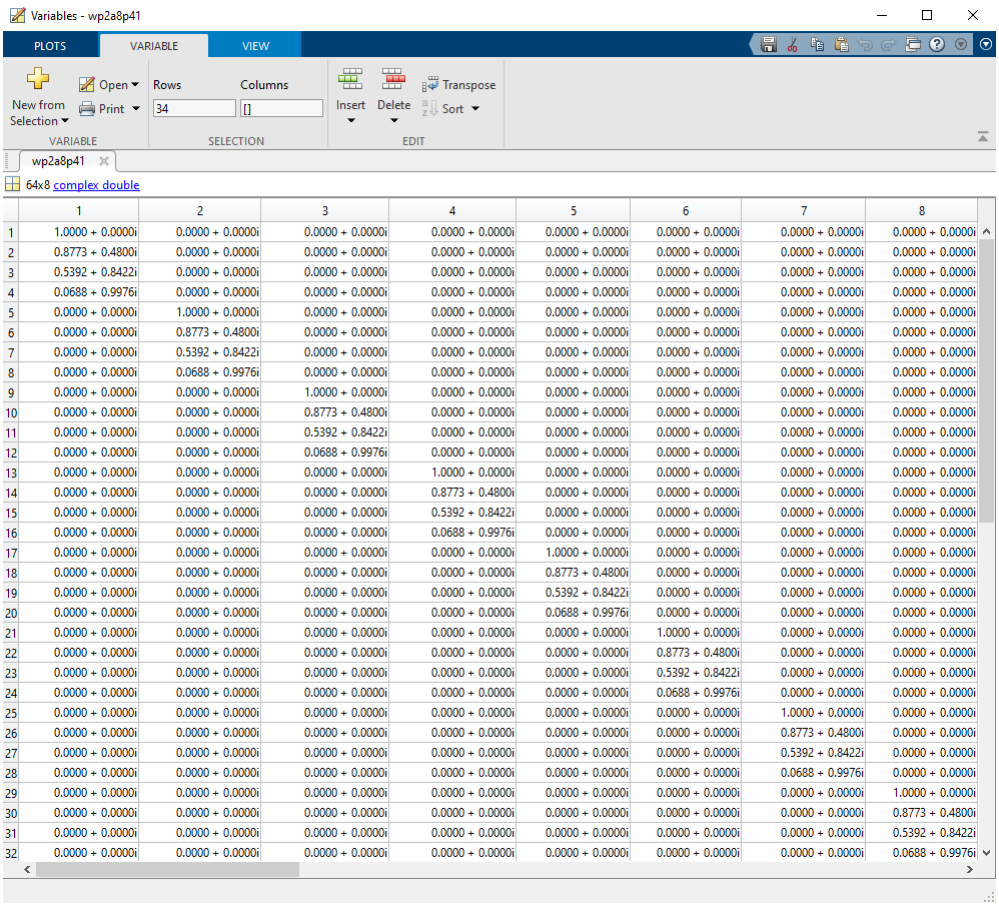

Figure 5.1: The antenna weight calculation for 8 CSI ports, (4,1) codebook

As shown in the figure, antenna elements 0-3 are used to transmit CSI-RS of antenna port 0 (CSI-RS 0), while antenna elements 4-7 are used to transmit CSI-RS 1, and so on. If

the digital tilt is set to 0, all antennas will have the same weight. This conclusion holds for all selected codebooks except 8 ports (2,2) codebook.

Step 2: Map the W_{p2a} matrix to the antenna array with 32 antenna elements.

Step 3: Combine the antenna array with the steering vector of the beam simulation system, and then derived beamforming gain, which is used to calculate the gap.

Step 4: Calculate the gap between the B5 (boresight direction) port and the other output ports.

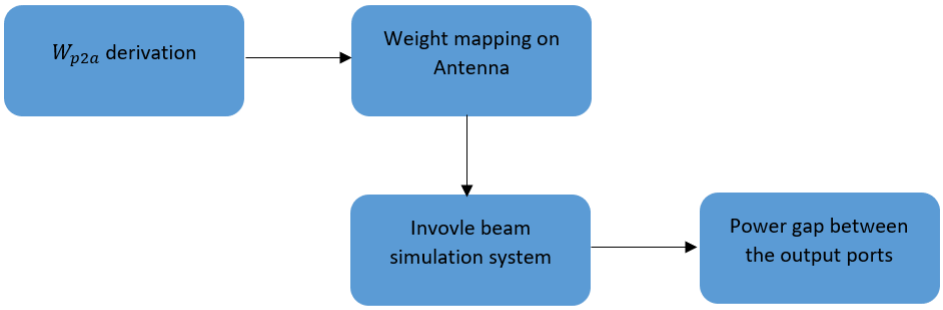

Figure 5.2: Simulation flowchart to calculate the gap between the B5 (boresight direction) port and the other output ports of beam simulation system

5.2 Simulation Result

Firstly, the physical angles of measured output ports are calculated by Equation 3.1. The calculation results are shown in Table 5.1. For each output port, the data observed on the spectrum analyzer are the signal power received by the UE at these locations. The simulation results of each CSI-RS configuration are shown in Tables 5.2-5.5. In fact, for most selected CSI-RS codebooks, the theoretical results for each antenna port are the same. Because in this thesis, the antenna elements are connected with the input ports of the beam simulation system by using cables. The physical distance between the antennas assigned to different antenna ports has no effect on the results. On the other hand, CSI-RS can be used to support the assessment of beam simulation system because of the consistency of antenna ports. The 8 ports (2,2) codebook is the exception here, because, for this codebook, the weight design of ports 0-3 is different from the weight design of ports 4-7.

Table 5.1: The physical angle of each position

Output port	Horizontal position (degree)	Vertical position (degree)
B1 Left	-25.68	0
B2 Up Left	-25.68	9.30
B4 Down	0	-9.30
B5 Boresight	0	0
B6 Up	0	9.30
B9 Right	25.68	0
B10 Up Right	25.68	9.30
B13 Very Left/Right	59.90	0

Table 5.2: Simulation results of antenna port 0-7, 8 CSI ports, (4,1) codebook

Output port	Theoretical gain(dB)	Gap to B5(dB)
B1 Left	10.63	0
B2 Up Left	-0.18	-10.81
B4 Down	4.36	-6.27
B5 Boresight	10.63	0
B6 Up	-0.18	-10.81
B9 Right	10.63	0
B10 Up Right	-0.18	-10.81
B13 Very Left/Right	10.63	0

Table 5.3: Simulation results of antenna port 0-3, 8 CSI ports, (2,2) codebook

Output port	Theoretical gain(dB)	Gap to B5(dB)
B1 Left	11.13	0.13
B2 Up Left	5.56	-5.44
B4 Down	9.97	-1.03
B5 Boresight	11.00	0
B6 Up	5.43	-5.57
B9 Right	3.03	-7.97
B10 Up Right	-2.54	-13.54
B13 Very Left/Right	3.78	-7.22

Table 5.4: Simulation results of antenna port 4-7, 8 CSI ports, (2,2) codebook

Output port	Theoretical gain(dB)	Gap to B5(dB)
B1 Left	3.03	-7.97
B2 Up Left	-2.54	-13.54
B4 Down	9.97	-1.03
B5 Boresight	11.00	0
B6 Up	5.43	-5.57
B9 Right	11.13	0.13
B10 Up Right	5.56	-5.44
B13 Very Left/Right	3.78	-7.22

Table 5.5: Simulation results of antenna port 0-15, 16 CSI ports, (4,2) codebook

Output port	Theoretical gain(dB)	Gap to B5(dB)
B1 Left	5.75	0
B2 Up Left	0.17	-5.58
B4 Down	4.71	-1.04
B5 Boresight	5.75	0
B6 Up	0.17	-5.58
B9 Right	5.75	0
B10 Up Right	0.17	-5.58
B13 Very Left/Right	5.75	0

The simulation results for the CSI 32 ports, (4,4) codebook do not need to be presented with the help of a table, since the beamforming gain is zero in all directions for each antenna port. Because only one antenna element is assigned to each antenna port and the antenna element is assumed to be omnidirectional in this thesis. The beamforming gain image of different CSI-RS codebooks can be easily observed from the simulation results. For example, for the 8 ports (4,1) codebook. The gain of the CSI-RS signal is omnidirectional in the horizontal direction, but the gain varies with vertical angle. Because the four antenna elements assigned to each antenna port are arranged vertically. A graphical representation of the antenna allocation is shown in Fig. 5.3. The simulation results give a preliminary image of the directivity pattern. For example, which directions should have high beamforming gain, and which directions should have the same gain so the measurements are expected to give the same result.

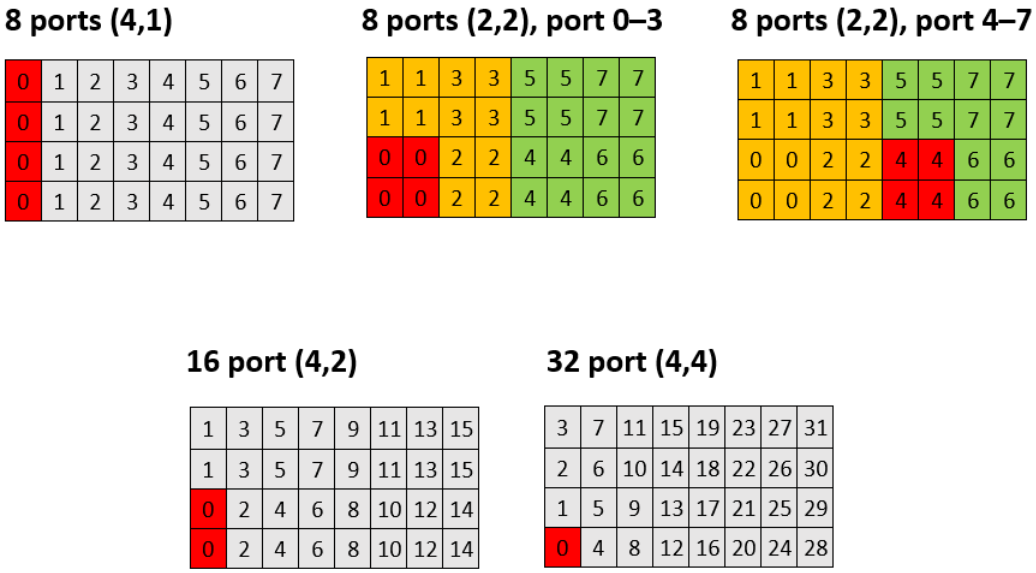

Figure 5.3: Graphical representation of the antenna allocation

6

Measurement Results

After getting the simulation results in the previous chapter, the report has reached the measurements part of this thesis work. For the selected CSI-RS codebook configurations, the laboratory test results are summarized in this chapter. Added to that, a comparison study between simulation and measurement results is introduced to assess the validity of beam simulation system. The 8 ports (4,1) codebook, 8 ports (2,2) codebook, 16 ports (4,2) codebook, and 32 ports (4,4) codebook were measured in this thesis.

6.1 Lab Measurement

When the base station starts transmitting data, the CCN can be remotely controlled through the Citrix workstation to select which output port of beam simulation system will be measured. By moving the UE and Spectrum analyzer to the different output ports. This operation corresponds to the user moving to different locations in field testing. As shown in Fig. 6.1, the eight circles correspond to the eight output ports to be measured. To measure the received signal power in that direction, move the UE and spectrum analyzer to the center of the circle. The power per resource element (PPRE) of the signal will then be displayed on the spectrum analyzer.

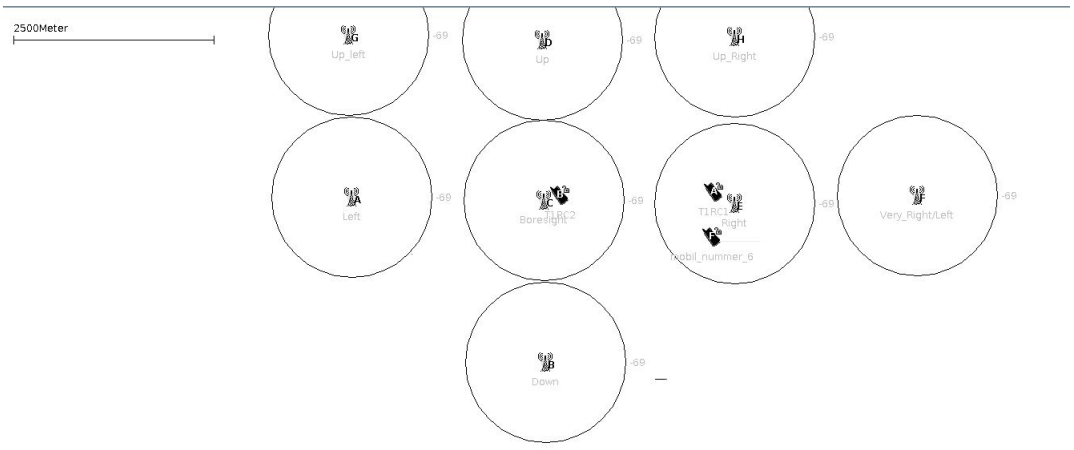

Figure 6.1: CCN interface with representatives of directions and UE

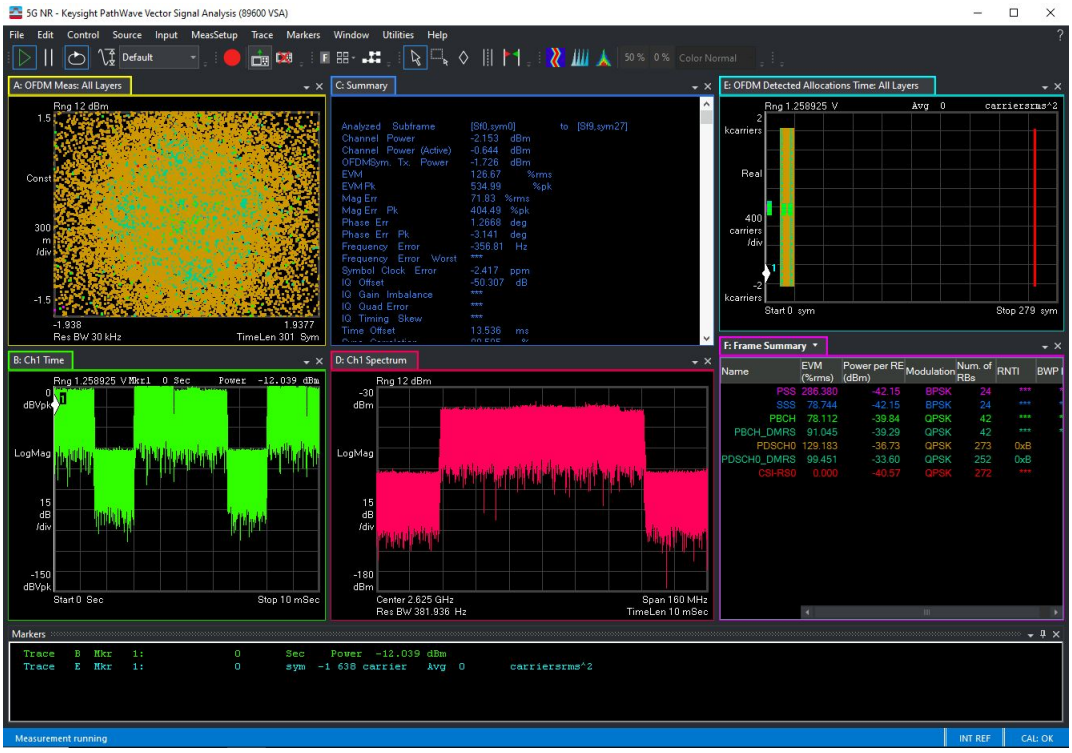

Figure 6.2: Spectrum analyzer interface, the PPRE can be observed on "Frame summary"

6.2 Measurement Result and Comparison Study

As the core part of this thesis, the evaluation of this beam simulation system can be carried out after the comparison study. If for a specific output port and antenna port, a large deviation between the measurement result and the simulation result is found, it means that there may be problems with the intermediate part of the input port and the output port. Components connected to this set of antenna ports and output ports provide incorrect phase shift. This assessment method can effectively narrow the scope of fault search and does not require the development of special test signals and methods. Evaluation can be conducted using existing CSI-RS to save the cost of design and time.

For the comparison study, we commented on deviations based on two borders that are green and red border. For MIMO testing, We usually have tolerance of ± 1 dB. If the deviation between the measurement value and the simulation value is less than 1 dB, the result is confirmed as perfect. If the deviation between the measurement value and the simulation value is greater than 1 dB and less than 2 dB. We need to mark the input and output ports corresponding to this result. In future testing, when the combination of these input and output ports is involved, it is necessary to consider adding a compensation value to it to deal with this deviation. In this case, the beam simulation system is still recognized to be correct, although there is an obvious error. If the deviation between the measurement result and the theoretical value is beyond 2 dB, the beam simulation system is considered faulty. The corresponding input and output ports should be marked because the faulty components may be in the intermediate circuit between these input and output ports.

The measurement of 32 ports (4,4) codebook is done as the first stage of measurement. The spectrum analyzer displayed the same result in every direction for every antenna port. After measurement, the measured PPRE is around -56 dBm and the deviations are less

than 1 dB for every CSI-RS signal and direction. The beam simulation system proved to work as expected with only one input antenna element. After that, the measurement of selected CSI-RS configurations is conducted and the results are shown in Tables 6.1-6.16.

6.2.1 Measurement result, 8 CSI ports, (4,1)

Table 6.1: Measurement results of antenna port 0-1, 8 CSI ports, (4,1) codebook, and comparison with the simulation results

Output port	PPRE(dBm)	Gap to B5(dB)	Simulation(dB)	Deviation(dB)
B1 Left	-45.97	0.55	0	0.55
B2 Up Left	-58.08	-11.56	-10.81	-0.75
B4 Down	-51.31	-4.79	-6.27	1.48
B5 Boresight	-46.52	0	0	0
B6 Up	-57.26	-10.74	-10.81	0.07
B9 Right	-46.28	0.24	0	0.24
B10 Up Right	-57.45	-10.93	-10.81	-0.12
B13 Very Left/Right	-46.47	0.05	0	0.05

By comparing the PPRE with the simulation results, the deviation between the actual performance and the ideal performance of the beam simulation system can be obtained. For antenna ports 00 and 01 of 8 CSI, (4,1) codebook (Table 6.1), the maximum deviation 1.48 dB appears at the B4 output port. This deviation is not within the ideal range, but it is feasible for compensation to counteract this error in future testing.

Table 6.2: Measurement results of antenna port 2-3, 8 CSI ports, (4,1) codebook, and comparison with the simulation results

Output port	PPRE(dBm)	Gap to B5(dB)	Simulation(dB)	Deviation(dB)
B1 Left	-46.17	-0.07	0	-0.07
B2 Up Left	-57.54	-11.44	-10.81	-0.63
B4 Down	-50.49	-4.39	-6.27	1.88
B5 Boresight	-46.10	0	0	0
B6 Up	-56.80	-10.70	-10.81	0.11
B9 Right	-46.49	-0.39	0	-0.39
B10 Up Right	-56.98	-10.88	-10.81	-0.07
B13 Very Left/Right	-46.12	-0.02	0	-0.02

For antenna ports 02 and 03 of 8 CSI, (4,1) codebook (Table 6.2), the maximum deviation 1.88 dB appears at the B4 output port. The deviation of other output ports is less than 1 dB.

Table 6.3: Measurement results of antenna port 4-5, 8 CSI ports, (4,1) codebook, and comparison with the simulation results

Output port	PPRE(dBm)	Gap to B5(dB)	Simulation(dB)	Deviation(dB)
B1 Left	-45.79	0.23	0	0.23
B2 Up Left	-58.32	-12.30	-10.81	-1.49
B4 Down	-51.75	-5.73	-6.27	0.54
B5 Boresight	-46.02	0	0	0
B6 Up	-57.78	-11.76	-10.81	-0.95
B9 Right	-46.14	-0.12	0	-0.12
B10 Up Right	-57.64	-11.62	-10.81	-0.81
B13 Very Left/Right	-46.53	-0.51	0	-0.51

For antenna ports 04 and 05 of 8 CSI, (4,1) codebook (Table 6.3), the maximum deviation 1.49 dB appears at the B2 output port. The deviation of other output ports is less than 1 dB.

Table 6.4: Measurement results of antenna port 6-7, 8 CSI ports, (4,1) codebook, and comparison with the simulation results

Output port	PPRE(dBm)	Gap to B5(dB)	Simulation(dB)	Deviation(dB)
B1 Left	-45.90	0.56	0	0.56
B2 Up Left	-57.99	-11.53	-10.81	-0.72
B4 Down	-51.45	-4.99	-6.27	1.28
B5 Boresight	-46.46	0	0	0
B6 Up	-57.34	-10.88	-10.81	-0.07
B9 Right	-45.21	1.25	0	1.25
B10 Up Right	-57.48	-11.02	-10.81	-0.21
B13 Very Left/Right	-46.04	0.42	0	0.42

For antenna ports 06 and 07 of 8 CSI, (4,1) codebook (Table 6.4), the maximum deviation 1.28 dB appears at the B4 output port. The deviation of other output ports is less than 1 dB expect B9 (1.25 dB).

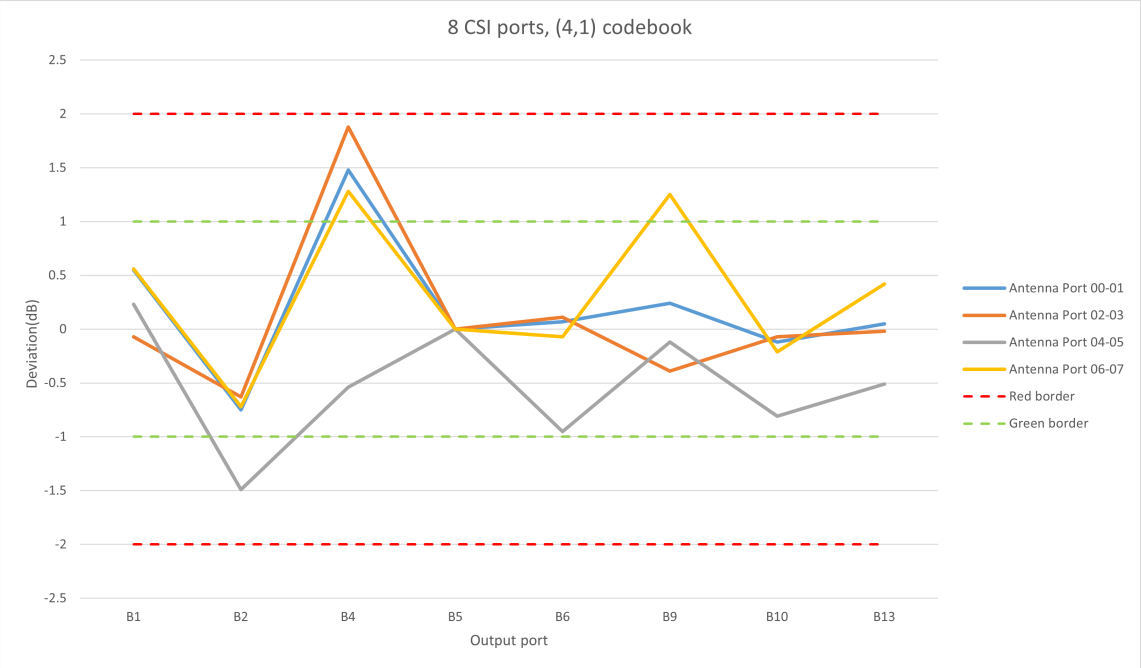

Figure 6.3: For each output port, the deviation between the simulation result and the measurement result, 8 CSI ports, (4,1) codebook

For 8 ports (4,1) codebook, the range of deviation is 0.05 to 1.88 dB. The largest deviation 1.88 dB is observed on the B4 output port (Down) and the corresponding antenna ports are 02 and 03. Based on this conclusion, it can be confirmed that when the B2 output port value of the beam simulation system is determined by the input ports A16-A19 (Antenna port 4) or A20-A23 (Antenna port 5), the compensation value is needed to intervene to offset this deviation. Meanwhile, when the value of the B4 output port depends on A0-A3 or A4-A7 or A8-A11 or A12-A15 or A24-A27 or A28-A31, the compensation value is needed to intervene to offset this deviation. When the B9 output depends on A24-A27 or A28-A31, the compensation value is needed to intervene to offset this deviation.

6.2.2 Measurement result, 8 CSI ports, (2,2)

Table 6.5: Measurement results of antenna port 0-1, 8 CSI ports, (2,2) codebook, and comparison with the simulation results

Output port	PPRE(dBm)	Gap to B5(dB)	Simulation(dB)	Deviation(dB)
B1 Left	-45.38	0.7	0.13	0.57
B2 Up Left	-51.49	-5.41	-5.44	0.03
B4 Down	-46.54	-0.51	-1.03	0.52
B5 Boresight	-46.08	0	0	0
B6 Up	-51.76	-5.68	-5.57	0.11
B9 Right	-53.79	-7.71	-7.97	0.26
B10 Up Right	-59.01	-12.93	-13.54	0.61
B13 Very Left/Right	-52.96	-6.88	-7.22	0.34

For antenna ports 00 and 01 of 8 CSI, (2,2) codebook (Table 6.5), The deviation of all output ports is less than 1 dB.

Table 6.6: Measurement results of antenna port 2-3, 8 CSI ports, (2,2) codebook, and comparison with the simulation results

Output port	PPRE(dBm)	Gap to B5(dB)	Simulation(dB)	Deviation(dB)
B1 Left	-45.45	0.13	0.13	0
B2 Up Left	-51.61	-6.03	-5.44	-0.59
B4 Down	-46.06	-0.48	-1.03	0.55
B5 Boresight	-45.58	0	0	0
B6 Up	-51.28	-5.70	-5.57	-0.13
B9 Right	-54.12	-8.54	-7.97	-0.57
B10 Up Right	-59.32	-13.74	-13.54	-0.20
B13 Very Left/Right	-52.32	-6.74	-7.22	0.48

For antenna ports 02 and 03 of 8 CSI, (2,2) codebook (Table 6.6), The deviation of all output ports is less than 1 dB.

Table 6.7: Measurement results of antenna port 4-5, 8 CSI ports, (2,2) codebook, and comparison with the simulation results

Output port	PPRE(dBm)	Gap to B5(dB)	Simulation(dB)	Deviation(dB)
B1 Left	-53.41	-7.49	-7.93	0.48
B2 Up Left	-58.97	-13.05	-13.54	0.49
B4 Down	-46.36	-0.44	-1.03	0.59
B5 Boresight	-45.92	0	0	0
B6 Up	-51.61	-5.69	-5.57	-0.12
B9 Right	-45.63	0.29	0.13	0.16
B10 Up Right	-50.97	-5.05	-5.44	0.39
B13 Very Left/Right	-53.63	-7.71	-7.22	-0.49

For antenna ports 04 and 05 of 8 CSI, (2,2) codebook (Table 6.7), The deviation of all output ports is less than 1 dB.

Table 6.8: Measurement results of antenna port 6-7, 8 CSI ports, (2,2) codebook, and comparison with the simulation results

Output port	PPRE(dBm)	Gap to B5(dB)	Simulation(dB)	Deviation(dB)
B1 Left	-53.87	-8.34	-7.93	-0.41
B2 Up Left	-58.30	-12.77	-13.54	0.77
B4 Down	-46.08	-0.55	-1.03	0.48
B5 Boresight	-45.53	0	0	0
B6 Up	-50.92	-5.39	-5.57	0.18
B9 Right	-45.80	-0.30	0.13	-0.17
B10 Up Right	-51.12	-5.59	-5.44	-0.15
B13 Very Left/Right	-52.78	-7.25	-7.22	-0.03

For antenna ports 06 and 07 of 8 CSI, (2,2) codebook (Table 6.8), The deviation of all output ports is less than 1 dB.

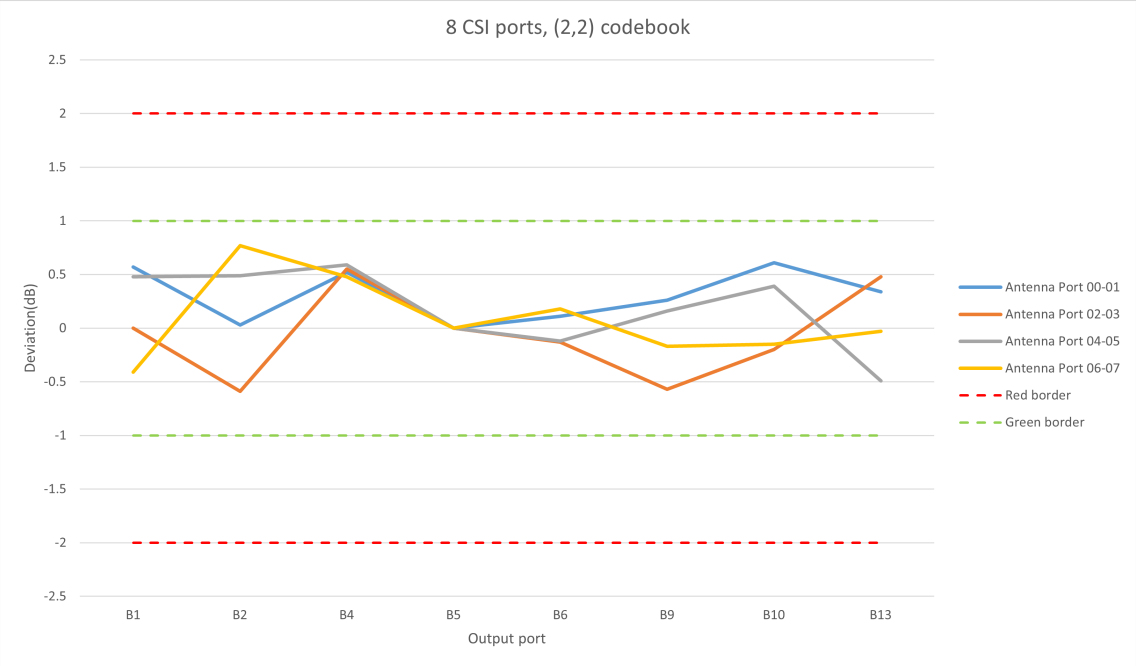

Figure 6.4: For each output port, the deviation between the simulation result and the measurement result, 8 CSI ports, (2,2) codebook

For 8 ports (2,2) codebook, the range of deviation (absolute value) is 0.03 to 0.77 dB. The largest deviation 0.77 dB is observed on the B2 port (Up Left). The beam simulation system has good performance for this CSI-RS configuration.

6.2.3 Measurement result, 16 CSI ports, (4,2)

Table 6.9: Measurement results of antenna port 0-1, 16 CSI ports, (4,2) codebook, and comparison with the simulation results

Output port	PPRE(dBm)	Gap to B5(dB)	Simulation(dB)	Deviation(dB)
B1 Left	-50.73	1.00	0	1.00
B2 Up Left	-56.56	-4.83	-5.58	-0.75
B4 Down	-52.11	-0.38	-1.04	0.66
B5 Boresight	-51.73	0	0	0
B6 Up	-57.42	-5.69	-5.58	-0.11
B9 Right	-50.99	0.74	0	0.74
B10 Up Right	-56.28	-4.55	-5.58	1.03
B13 Very Left/Right	-51.24	0.49	0	0.49

For antenna ports 00 and 01 of 16 CSI, (4,2) codebook (Table 6.9), the maximum deviation 1.03 dB appears at the B2 output port. The deviation of other output ports is less than 1 dB expect B1 (1.00 dB).

Table 6.10: Measurement results of antenna port 2-3, 16 CSI ports, (4,2) codebook, and comparison with the simulation results

Output port	PPRE(dBm)	Gap to B5(dB)	Simulation(dB)	Deviation(dB)
B1 Left	-50.72	0.35	0	0.35
B2 Up Left	-56.85	-5.78	-5.58	-0.20
B4 Down	-51.43	-0.36	-1.04	0.68
B5 Boresight	-51.07	0	0	0
B6 Up	-56.68	-5.61	-5.58	-0.03
B9 Right	-51.05	0.02	0	0.02
B10 Up Right	-56.54	-5.47	-5.58	0.11
B13 Very Left/Right	-51.55	-0.48	0	-0.48

For antenna ports 02 and 03 of 16 CSI, (4,2) codebook (Table 6.10), The deviation of all output ports is less than 1 dB.

Table 6.11: Measurement results of antenna port 4-5, 16 CSI ports, (4,2) codebook, and comparison with the simulation results

Output port	PPRE(dBm)	Gap to B5(dB)	Simulation(dB)	Deviation(dB)
B1 Left	-50.94	0.23	0	0.23
B2 Up Left	-57.13	-5.96	-5.58	-0.38
B4 Down	-51.43	-0.26	-1.04	0.78
B5 Boresight	-51.17	0	0	0
B6 Up	-57.17	-6.00	-5.58	-0.42
B9 Right	-51.32	-0.15	0	-0.15
B10 Up Right	-56.90	-5.73	-5.58	-0.15
B13 Very Left/Right	-50.76	0.41	0	0.41

For antenna ports 04 and 05 of 16 CSI, (4,2) codebook (Table 6.11), The deviation of all output ports is less than 1 dB.

Table 6.12: Measurement results of antenna port 6-7, 16 CSI ports, (4,2) codebook, and comparison with the simulation results

Output port	PPRE(dBm)	Gap to B5(dB)	Simulation(dB)	Deviation(dB)
B1 Left	-50.87	-0.56	0	-0.56
B2 Up Left	-56.74	-6.42	-5.58	-0.85
B4 Down	-50.93	-0.62	-1.04	0.42
B5 Boresight	-50.31	0	0	0
B6 Up	-55.76	-5.45	-5.58	0.13
B9 Right	-51.16	-0.85	0	-0.85
B10 Up Right	-56.42	-6.11	-5.58	-0.53
B13 Very Left/Right	-50.92	-0.61	0	-0.61

For antenna ports 06 and 07 of 16 CSI, (4,2) codebook (Table 6.12), The deviation of all output ports is less than 1 dB.

Table 6.13: Measurement results of antenna port 8-9, 16 CSI ports, (4,2) codebook, and comparison with the simulation results

Output port	PPRE(dBm)	Gap to B5(dB)	Simulation(dB)	Deviation(dB)
B1 Left	-50.70	1.02	0	1.02
B2 Up Left	-56.36	-4.64	-5.58	0.94
B4 Down	-52.21	-0.49	-1.04	0.55
B5 Boresight	-51.72	0	0	0
B6 Up	-57.32	-5.60	-5.58	-0.02
B9 Right	-51.00	0.72	0	0.72
B10 Up Right	-56.12	-4.40	-5.58	1.18
B13 Very Left/Right	-51.16	0.56	0	0.56

For antenna ports 08 and 09 of 16 CSI, (4,2) codebook (Table 6.13), the maximum deviation 1.18 dB appears at the B10 output port. The deviation of other output ports is less than 1 dB expect B1 (1.02 dB).

Table 6.14: Measurement results of antenna port 10-11, 16 CSI ports, (4,2) codebook, and comparison with the simulation results

Output port	PPRE(dBm)	Gap to B5(dB)	Simulation(dB)	Deviation(dB)
B1 Left	-50.62	0.36	0	0.36
B2 Up Left	-56.63	-5.65	-5.58	-0.07
B4 Down	-51.42	-0.44	-1.04	0.60
B5 Boresight	-50.98	0	0	0
B6 Up	-56.56	-5.58	-5.58	0
B9 Right	-50.95	0.03	0	0.03
B10 Up Right	-56.37	-5.39	-5.58	0.19
B13 Very Left/Right	-51.48	-0.50	0	-0.50

For antenna ports 10 and 11 of 16 CSI, (4,2) codebook (Table 6.14), The deviation of all output ports is less than 1 dB.

Table 6.15: Measurement results of antenna port 12-13, 16 CSI ports, (4,2) codebook, and comparison with the simulation results

Output port	PPRE(dBm)	Gap to B5(dB)	Simulation(dB)	Deviation(dB)
B1 Left	-50.90	0.28	0	0.28
B2 Up Left	-56.76	-5.58	-5.58	0
B4 Down	-51.59	-0.41	-1.04	0.63
B5 Boresight	-51.18	0	0	0
B6 Up	-56.77	-5.59	-5.58	-0.01
B9 Right	-51.27	-0.09	0	-0.09
B10 Up Right	-56.58	-5.40	-5.58	0.18
B13 Very Left/Right	-50.71	0.47	0	0.47

For antenna ports 12 and 13 of 16 CSI, (4,2) codebook (Table 6.15), The deviation of all output ports is less than 1 dB.

Table 6.16: Measurement results of antenna port 14-15, 16 CSI ports, (4,2) codebook, and comparison with the simulation results

Output port	PPRE(dBm)	Gap to B5(dB)	Simulation(dB)	Deviation(dB)
B1 Left	-50.92	-0.54	0	-0.54
B2 Up Left	-56.43	-6.05	-5.58	-0.47
B4 Down	-51.02	-0.64	-1.04	0.40
B5 Boresight	-50.38	0	0	0
B6 Up	-55.63	-5.25	-5.58	0.33
B9 Right	-51.22	-0.84	0	-0.84
B10 Up Right	-56.40	-6.02	-5.58	-0.44
B13 Very Left/Right	-50.97	-0.59	0	-0.59

For antenna ports 14 and 15 of 16 CSI, (4,2) codebook (Table 6.16), The deviation of all output ports is less than 1 dB.

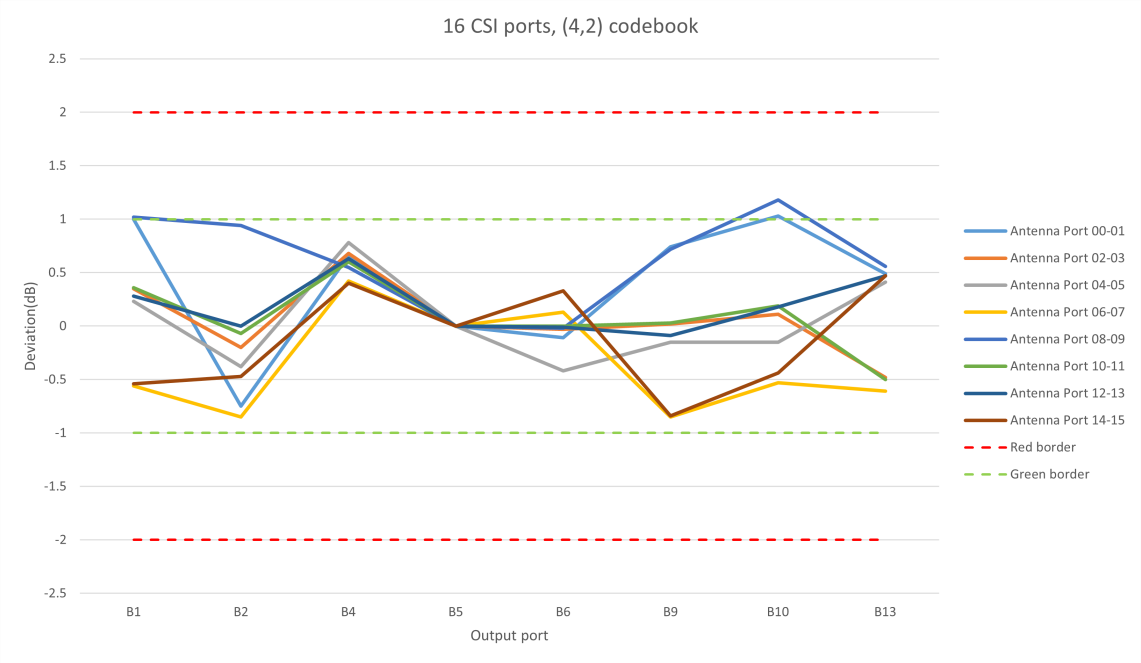

Figure 6.5: For each output port, the deviation between the simulation result and the measurement result, 16 CSI ports, (4,2) codebook

For 16 ports (4,2) codebook, the range of deviation is 0 to 1.18 dB. The largest deviation 1.18 dB is observed on the B10 port (Up Right) and the corresponding antenna ports are 08 and 09. Based on this comparison study, it can be confirmed that when the B1 output port value of the beam simulation system is determined by the input ports A0-A1 or A2-A3, the compensation value is needed to intervene to offset this deviation. Meanwhile, when the value of the B10 output port depends on A0-A1 or A2-A3 or A16-A17 or A18-A19, the compensation value is needed to intervene to offset this deviation.

6.3 Final Remarks

The conclusion is that the validity of this beam simulation system is verified when a deviation of less than 2 dB is considered acceptable. In future testing, when the signal is transmitted into following input ports and measured at following output ports, compensation values need to be involved.

1) Output B1, Input A0-A1 or A2-A3;

2) Output B2, Input A16-A19 or A20-A23;

3) Output B4, Input A0-A3 or A4-A7 or A8-A11 or A12-A15 or A24-A27 or A28-A31;

4) Output B9, Input A24-A27 or A28-A31;

5) Output B10, Input A0-A1 or A2-A3 or A16-A17 or A18-A19;

7

Conclusions and Future work

7.1 Conclusions

In this thesis, we have assessed the validity of a Butler matrix-based beam simulation system. This thesis covers the CSI-RS protocol and antenna mapping, and how we used CSI-RS as a tool to test the beam simulation system. The thesis also discussed the structure of the beamforming test system and the parameters of the device involved in the test system such as the AAS. A series of measurement and simulation plans were proposed and executed. The comparison study between the measurement results and the simulation results was presented as the core content of the thesis. For each configuration, the corresponding measurement and simulation results were introduced.

The CSI-RS is very useful for the assessment. Instead of developing a specific testing tool, we use existing resources. In addition, this is an innovative extension of the CSI-RS usage scenario. The characteristic of CSI-RS successfully helped us isolate the specific input and output ports of the beam simulation system so that we could locate the faulty components in a small range.

7.2 Future work

The purpose of this thesis was to draft an assessment method and verify the validity of the beam simulation system. Therefore, future work is to modify the assessment method to increase the efficiency of assessment. For example, optimize the scheme of the CSI-RS codebook selection to locate faulty components more precisely and reduce the time required for simulation and measurement. In addition, the assessment can be further extended to the component of beam simulation system. For example, if a component is confirmed as damaged, the exact phase offset of the damaged component can be derived through comparison study.

Bibliography

[1] Xingfeng Wu, Na Wang, Zhihua Zhang, Niels Kuster, and Weiming Wang. "Comparison tests and hand phantom standardization for multi-probe based MIMO OTA". In: *2016 IEEE 5th Asia-Pacific Conference on Antennas and Propagation (APCAP)*. 2016, pp. 321–322. DOI: 10.1109/APCAP.2016.7843223.

[2] Ya Jing, Zhu Wen, Hongwei Kong, Steve Duffy, and Moray Rumney. "Two-stage over the air (OTA) test method for MIMO device performance evaluation". In: *2011 IEEE International Symposium on Antennas and Propagation (APSURSI)*. 2011, pp. 71–74. DOI: 10.1109/APS.2011.5996385.

[3] Hongwei Kong, Zhu Wen, Ya Jing, and Michael Yau. "A compact millimeter wave (mmWave) mid-field over the air (OTA) RF performance test system for 5G massive MIMO devices". In: *2018 IEEE MTT-S International Wireless Symposium (IWS)*. 2018, pp. 1–4. DOI: 10.1109/IEEE-IWS.2018.8400995.

[4] Mamta Agiwal, Abhishek Roy, and Navrati Saxena. "Next Generation 5G Wireless Networks: A Comprehensive Survey". In: *IEEE Communications Surveys Tutorials* 18.3 (2016), pp. 1617–1655. DOI: 10.1109/COMST.2016.2532458.

[5] Hossein Khaleghi Bizaki. *MIMO Systems*. Rijeka: IntechOpen, 2011. DOI: 10.5772/610. URL: https://doi.org/10.5772/610.

[6] Rodrigo C. de Lamare. "Massive MIMO systems: Signal processing challenges and future trends". In: *URSI Radio Science Bulletin* 2013.347 (2013), pp. 8–20. DOI: 10.23919/URSIRSB.2013.7909827.

[7] Peter Butovitsch, David Astely, Thomas Chapman, Mattias Frenne, Henrik Asplund, Måns Hagström, Billy Hogan, George Jöngren, Jonas Karlsson, Fredric Kronestedt, Erik Larsson, and Farshid Ghasemzadeh. *Advanced Antenna Systems for 5G Network Deployments - Bridging the Gap Between Theory and Practice*. June 2020. ISBN: 9780128200469.

[8] Chia-Chan Chang, Ruey-Hsuan Lee, and Ting-Yen Shih. "Design of a Beam Switching/Steering Butler Matrix for Phased Array System". In: *IEEE Transactions on Antennas and Propagation* 58.2 (2010), pp. 367–374. DOI: 10.1109/TAP.2009.2037693.

[9] Peter von Butovitsch, David Astely, Christer Friberg, Anders Furuskär, Bo Göransson, Billy Hogan, Jonas Karlsson and Erik Larsson. *Advanced antenna systems for 5G network*. https://www.ericsson.com/en/reports-and-papers/white-papers/advanced-antenna-systems-for-5g-networks, Last accessed on 2022-8-2. 2018.

[10] Jaspreet Singh and Sudhir Ramakrishna. "On the Feasibility of Codebook-Based Beamforming in Millimeter Wave Systems With Multiple Antenna Arrays". In: *IEEE Transactions on Wireless Communications* 14.5 (2015), pp. 2670–2683. DOI: 10.1109/TWC.2015.2390637.

[11] Stefan Parkvall, Erik Dahlman, Anders Furuskar, and Mattias Frenne. "NR: The New 5G Radio Access Technology". In: *IEEE Communications Standards Magazine* 1.4 (2017), pp. 24–30. DOI: 10.1109/MCOMSTD.2017.1700042.

[12] Xuesong Cai, Yang Miao, Jinxing Li, Fredrik Tufvesson, Gert Frølund Pedersen, and Wei Fan. "Dynamic mmWave Channel Emulation in a Cost-Effective MPAC With Dominant-Cluster Concept". In: *IEEE Transactions on Antennas and Propagation* 70.6 (2022), pp. 4691–4704. DOI: 10.1109/TAP.2021.3137235.

[13] A. Paulraj, R. Nabar, and D. Gore. *Introduction to Space-Time Wireless Communications*. Cambridge University Press, 2003. ISBN: 9780521826150. URL: https://books.google.se/books?id=YQSsoPDfyngC.

[14] Wei Yu, Yihong Qi, Kefeng Liu, Yangguang Xu, and Jun Fan. "Radiated Two-Stage Method for LTE MIMO User Equipment Performance Evaluation". In: *IEEE Transactions on Electromagnetic Compatibility* 56.6 (2014), pp. 1691–1696. DOI: 10.1109/TEMC.2014.2320779.

[15] Peter von Butovitsch, David Astely, Anders Furuskär, Bo Göransson, Billy Hogan, Jonas Karlsson, and Erik Larsson. *Advanced antenna systems for 5G networks*. https://www.ericsson.com/en/reports-and-papers/white-papers/advanced-antenna-systems-for-5g-networks. Accessed: 2010-09-30.

[16] Thomas L. Marzetta. "Noncooperative Cellular Wireless with Unlimited Numbers of Base Station Antennas". In: *IEEE Transactions on Wireless Communications* 9.11 (2010), pp. 3590–3600. DOI: 10.1109/TWC.2010.092810.091092.

[17] J. Butler. "Beam-forming matrix simplifies design of electronically scanned antennas". In: *Electronic Design* 9 (1961), pp. 170–173.

[18] J. Blass. "Multidirectional antenna - A new approach to stacked beams". In: *1958 IRE International Convention Record*. Vol. 8. 1960, pp. 48–50. DOI: 10.1109/IRECON.1960.1150892.

[19] Erik Dahlman, Stefan Parkvall, and Johan Sköld. "Chapter 8 - Channel Sounding". In: *5G NR: the Next Generation Wireless Access Technology*. Ed. by Erik Dahlman, Stefan Parkvall, and Johan Sköld. Academic Press, 2018, pp. 133–152. ISBN: 978-0-12-814323-0. DOI: https://doi.org/10.1016/B978-0-12-814323-0.00008-9. URL: https://www.sciencedirect.com/science/article/pii/B9780128143230000089.

Appendix A

(Beam simulation system description, full version)

Table A.1: Beam simulation system description, full version

	B0	B1	B2	B3	B4	B5	B6	B7	B8	B9	B10	B11	B12	B13	B14	B15
A0	1	1	-i	1	1	1	-i	1	-i	-i	-1	-i	1	1	-i	1
A4	-i	-i	-1	-i	1	1	-i	1	1	1	-i	1	-1	-1	i	-1
A8	-1	-1	i	-1	1	1	-i	1	i	i	1	i	1	1	-i	1
A12	i	i	1	i	1	1	-i	1	-1	-1	i	-1	-1	-1	i	-1
A1	-i	1	1	-1	-i	1	1	-1	-1	-i	-i	i	-i	1	1	-1
A5	-1	-i	-i	i	-i	1	1	-1	-i	1	1	-1	i	-1	-1	1
A9	i	-1	-1	1	-i	1	1	-1	1	i	i	-i	-i	1	1	-1
A13	1	i	i	-i	-i	1	1	-1	i	-1	-1	1	i	-1	-1	1
A2	-1	1	i	1	-1	1	i	1	i	-i	1	-i	-1	1	i	1
A6	i	-i	1	-i	-1	1	i	1	-1	1	i	1	1	-1	-i	-1
A10	1	-1	-i	-1	-1	1	i	1	-i	i	-1	i	-1	1	i	1
A14	-i	i	-1	i	-1	1	i	1	1	-1	-i	-1	1	-1	-i	-1
A3	i	1	-1	-1	i	1	-1	-1	1	-1	i	i	i	1	-1	-1
A7	1	-i	i	i	i	1	-1	-1	i	1	-1	-1	-i	-1	1	1
A11	-i	-1	1	1	i	1	-1	-1	-1	i	-i	-i	i	1	-1	-1
A15	-1	i	-i	-i	i	1	-1	-1	-i	-1	1	1	-i	-1	1	1
A16	1	1	-i	1	1	1	-i	1	-i	-i	-1	-i	1	1	-i	1
A20	-i	-i	-1	-i	1	1	-i	1	1	1	-i	1	-1	-1	i	-1
A24	-1	-1	i	-1	1	1	-i	1	i	i	1	i	1	1	-i	1
A28	i	i	1	i	1	1	-i	1	-1	-1	i	-1	-1	-1	i	-1
A17	-i	1	1	-1	-i	1	1	-1	-1	-i	-i	i	-i	1	1	-1
A21	-1	-i	-i	i	-i	1	1	-1	-i	1	1	-1	i	-1	-1	1
A25	i	-1	-1	1	-i	1	1	-1	1	i	i	-i	-i	1	1	-1
A29	1	i	i	-i	-i	1	1	-1	i	-1	-1	1	i	-1	-1	1
A18	-1	1	i	1	-1	1	i	1	i	-i	1	-i	-1	1	i	1
A22	i	-i	1	-i	-1	1	i	1	-1	1	i	1	1	-1	-i	-1
A26	1	-1	-i	-1	-1	1	i	1	-i	i	-1	i	-1	1	i	1
A30	-i	i	-1	i	-1	1	i	1	1	-1	-i	-1	1	-1	-i	-1
A19	i	1	-1	-1	i	1	-1	-1	1	-1	i	i	i	1	-1	-1
A23	1	-i	i	i	i	1	-1	-1	i	1	-1	-1	-i	-1	1	1
A27	-i	-1	1	1	i	1	-1	-1	-1	i	-i	-i	i	1	-1	-1
A31	-1	i	-i	-i	i	1	-1	-1	-i	-1	1	1	-i	-1	1	1

Table A.2: The direction represented by each outlet

Output port	Direction
B0	Down Left
B1	Left
B2	Up Left
B3	Very Up Left
B4	Down
B5	Boresight
B6	Up
B7	Very Up
B8	Down Right
B9	Right
B10	Up Right
B11	Very Up Right
B12	Down Very Right/Left
B13	Very Right/Left
B14	Up Very Right/Left
B15	Very Up Very Right/Left